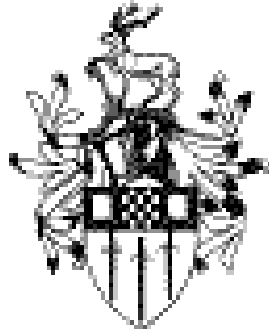


NEUTRON CONTAMINATION IN A RADIOTHERAPY MAZE



Mary PW Chin
Department of Physics
University of Surrey

A dissertation submitted as partial fulfilment of the degree of
Master of Science in Medical Physics

1999

Abstract

This work attempts to investigate neutron contamination in a radiotherapy maze that houses a high-energy medical linear accelerator. While electrons and/or photons from the linac are destined for therapeutic effects by destroying cancerous cells, the production of neutrons which are hazardous is unintended but inevitable. This work attempts to quantify the degree of this contamination. The variation of neutron fluence in the treatment room, the variation of neutron dose along the passage of the maze, the changes in neutron energy distribution as the neutrons traverse the treatment head and the passage of the maze will be quantified using Monte Carlo simulation. Data will be compared with estimations from empirical formulae developed by McCall, for neutron fluence, and Kersey, for neutron dose equivalent. The presence of secondary photons will also be briefly demonstrated. To take advantage of the flexibility computer simulation offers, modified maze designs will be explored by comparing a double-bended maze with a single-bended one, and by comparing bunkers of varying heights.

downloaded from www.marychm.org

Acknowledgements

It has been a year of many blessed encounters. Dr Spyrou's encouragement and confidence nourished every moment of the course - he is indeed the most supportive mentor I have ever met. Sue's help and friendship made such a difference to my stay in England. The special people in our class made the classroom experience wonderful.

I am most grateful to be granted the International Development Shared Scholarship Scheme, which made my attendance of the course possible.

I thank the people who contributed directly to this dissertation project. Once again, Dr Spyrou, whose supervision I enjoyed. Also Dr Robert Price, who answered via email some of my questions about MCNP. A few others helped briefly.

Yet another moment of grace, this is also a time to remember those who took part in my first faltering steps. Dr Sivananthan and Dr Pathmanathan gave orthopaedic and paediatric care respectively. Sister Hermine was the physiotherapist, who remains an inspiration. All medical treatment was founded on papa's tremendous patience and commitment. Greater difficulty came from my primary school days which I miraculously survived, adding to mama's pain more than she could bear. This work brings the course to its finale. It is dedicated to papa and mama. May it be a delight.

TABLE OF CONTENTS

1. The Hazard Defined	
• Neutron Production	1
• Neutron Interactions	11
• Residual Activities	12
2. Shielding the Hazard	
• The Material	14
• The Design	17
3. Quantifying the Hazard I: The Approach	
• Deterministic Approach	19
• A Deterministic Simulation	19
• Monte Carlo Approach	26
• MCNP	27
4. Quantifying the Hazard II: Data & Analysis	
• Neutron Dose	33
• Neutron Fluence	39
• Neutron Energy Distribution	42
• Secondary Photons	45
5. Quantifying the Hazard III: Errors & Reliability	
• Variance Reduction	47
• The 10 Statistical Checks	52
• The 2 dangers	56
• Reproducibility	59
• Neutron Cross Sections	59
• Fluence-to-Dose Conversion	60
• Limitations of the Model	62
6. Conclusion	65
7. References	
8. Appendices	
• Program Listing of Deterministic Simulation	
• A Sample MCNP Input	

Chapter 1. THE HAZARD DEFINED

Neutron Production

In a medical electron accelerator installation, electrons and photons are the particles intentionally produced in order to destroy cancerous cells, thus producing the desired therapeutic effect. When these particles impinge on surrounding materials assembled in the treatment head, the electrons may undergo electro-neutron ($e,e'n$) interactions and the photons may undergo photoneutron (γ,n) interactions. The former is about 100 times less probable than the latter. Both types of interaction produce neutrons that are not intended but come as a by-product. Shielding is necessary so that the patient, the staff and the public are not exposed to any accidental 'neutron therapy'.

Sources of neutron contamination in the treatment head include walls of vacuum chamber, walls of waveguide, x-ray target, beam extractor, filters, collimators, transmission ionisation chambers and light localizers. A treatment head is shown in Figure 1-1.

Apart from the treatment head, other sources of photoneutrons include the patient, the air and the walls of the bunker. The problem is further aggravated if high density materials, usually metal, are embedded in the walls - intended for shielding photons but at the same time act as sources of photoneutrons as well. The neutron dose equivalent outside the bunker would be higher if the barriers contain lead or steel compared to the case where pure concrete barriers are used. The recent excitement of conformal therapy brings in the multileaf collimator, usually made of lead, which can be another source of photoneutrons as well. A treatment head with multileaf collimator installed is shown in Figure 1-2.

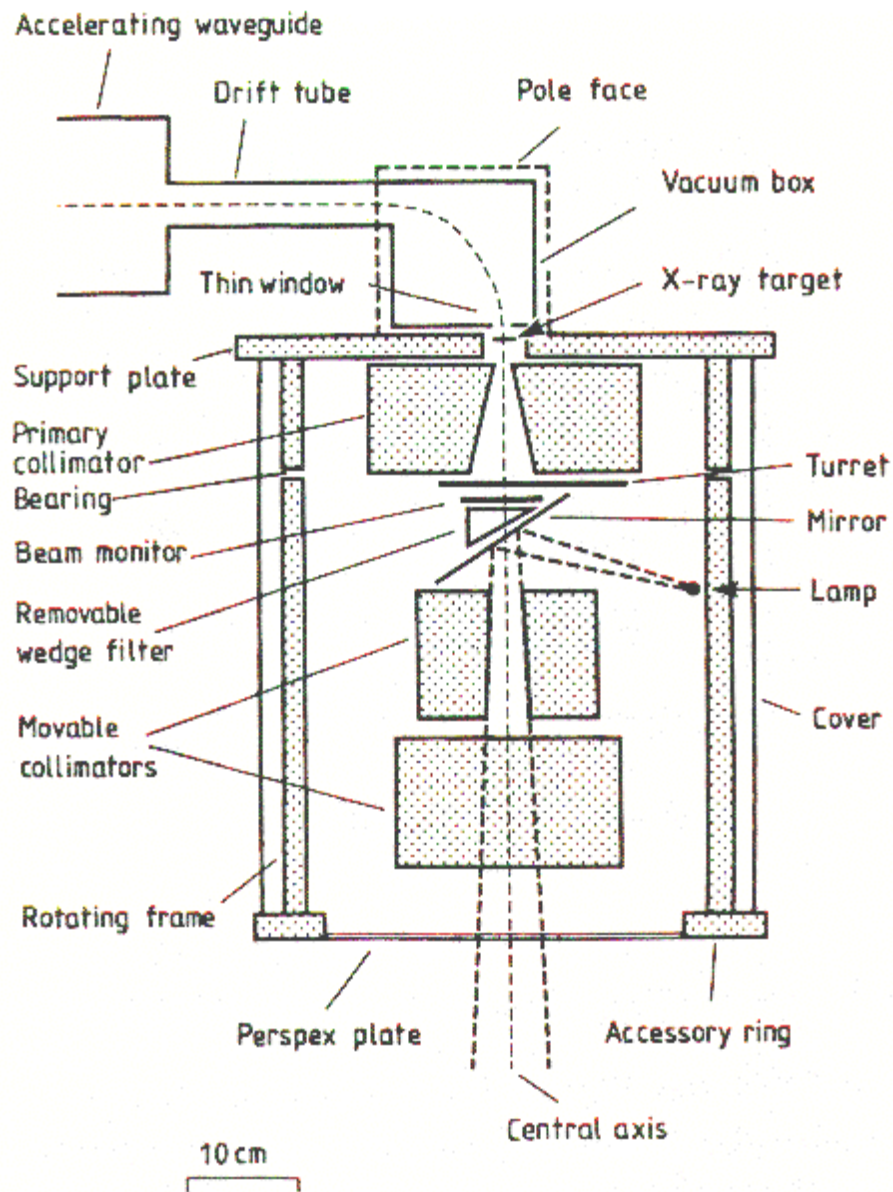


Figure 1-1. The treatment head of a medical linear accelerator. [GRE 85]

6.9

downloaded

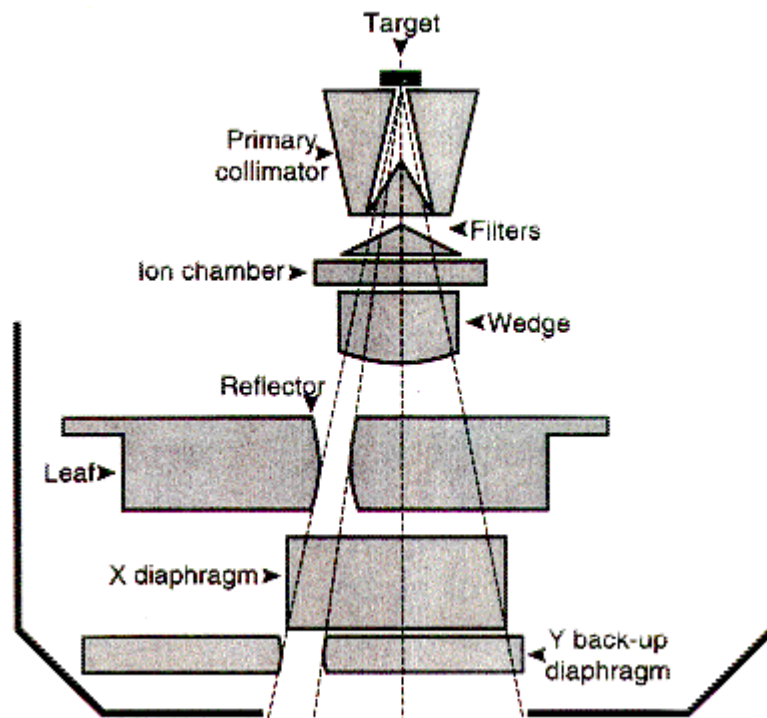


Figure 1-2. A treatment head with multileaf collimator installed. [GRE 85]

Photoneutron production is governed by the neutron separation energy and the photoneutron cross-section. The neutron separation energy is the threshold energy that must be overcome in order for the interaction to occur. The neutron separation energies for a range of isotopes are calculated and tabulated in Table 1-1. It shows that even at photon energies below 10 MeV, lead and tungsten are capable of producing neutrons. At the photon energies between 10 and 20 MeV, more other materials are likely to undergo the (γ, n) interaction while lead and tungsten are even capable of producing neutron pairs, as shown in Table 1-2.

Isotopes of interest include ^1H , ^{16}O , ^{12}C and ^{14}N in the patient's body, ^{16}O and ^{14}N in the air, ^{184}W , ^{208}Pb and ^{27}Al in the treatment head and treatment accessories, also ^1H , ^{16}O , ^{28}Si , ^{40}Ca and ^{12}C in the concrete walls. ^{10}B and ^{11}B are sometimes used for maze lining to shield against neutrons.

Once the interaction threshold is overcome, neutrons emerge with kinetic energies which can be calculated as well. This is tabulated in Table 1-3.

Table 1-1. Photo-neutron production by (γ, n) interaction.

ELEMENT	Z	A Of TARGET NUCLIDE	(γ, n) THRESHOLD (MeV)	A of PRODUCT NUCLIDE	Half-life
O	8	16	15.7	15	122 s
C	6	12	18.7	11	20.4 m
N	7	14	10.6	13	9.96 m
Al	13	27	13.1	26	.72 My
W	74	182	8.1	181	121 d
		183	6.2	182	Stable
		184	7.4	183	Stable
		186	5.8	184	Stable
Pb	82	206	8.1	205	15 My
		207	6.7	206	Stable
		208	7.4	207	5.8 h
Si	14	28	17.2	27	4.13 s
Ca	20	40	15.6	39	.86 s
Mg	12	24	16.5	23	11.3 s
Fe	26	54	13.4	53	Stable
		56	11.2	55	2.7 y
Na	11	23	12.4	22	2.60 y
K	19	39	13.1	38	7.61 m
B	5	10	8.4	9	Stable
B	5	11	7.2	10	Stable

Table 1-2. Photo-neutron production by ($\gamma, 2n$) interaction.

ELEMENT	Z	A of TARGET NUCLIDE	($\gamma, 2n$) THRESHOLD (MeV)	A of PRODUCT NUCLIDE	Half-life
O	8	16	28.89	14	71 s
C	6	12	31.84	10	19 s
N	7	14	30.62	12	11 ms
Al	13	27	24.42	25	7.18 s
W	74	184	13.60	182	Stable
Pb	82	208	15.30	206	Stable
Si	14	28	30.49	26	2.21 s
Mg	12	24	29.68	22	2.86
Fe	26	56	20.50	54	Stable

Table 1-3. Kinetic energies of emerging neutrons.

ELEMENT	INCIDENT PHOTON ENERGY (MeV)			
	10	15	20	25
	Kinetic Energy of Neutrons (MeV)			
O	-	-	4.3	9.3
C	-	-	1.3	6.3
N	-	4.4	9.4	14.4
Al	-	1.9	6.9	11.9
W	2.6	7.6	12.6	17.6
Pb	2.6	7.6	12.6	17.6
Si	-	-	2.8	7.8
Ca	-	-	4.4	9.4
Mg	-	-	3.5	8.5
Fe	-	3.8	8.8	13.8
Na	-	2.6	7.6	12.6
K	-	1.9	6.9	11.9
B	1.6	6.6	11.6	16.6
B	17.2	22.2	27.2	32.2

When a photoneutron interaction takes place, one or more neutrons may be produced. Therefore the photoneutron production cross-section is the sum of $\sigma(\gamma,1n)$, $\sigma(\gamma,2n)$, $\sigma(\gamma,3n)$ and so on, where $\sigma(\gamma,1n)$ usually contributes most. The photoneutron yield cross-section, on the other hand, is the sum of $\sigma(\gamma,1n)$, $2\sigma(\gamma,2n)$, $3\sigma(\gamma,3n)$, etc. When a single neutron is produced, it may be accompanied by alphas or protons. The same is true for $\sigma(\gamma,2n)$, $\sigma(\gamma,3n)$, etc. Therefore, $\sigma(\gamma,1n)$ itself is a sum of $\sigma(\gamma,n)$, $\sigma(\gamma,n\alpha)$ and $\sigma(\gamma,np)$.

The (γ,xn) and (γ,n) cross sections for ^{12}C and ^{16}O , copper and ^{208}Pb are given in Figures 1-3 and 1-4.

The photon absorption cross-section is different for each isotope and is a function of photon energy. The relation takes the form of a bell shape, where there is a giant resonance at which the photon absorption cross-section is maximum. If the giant resonance is broad and if the incident photon energy is located near the resonance, many particles will be emitted.

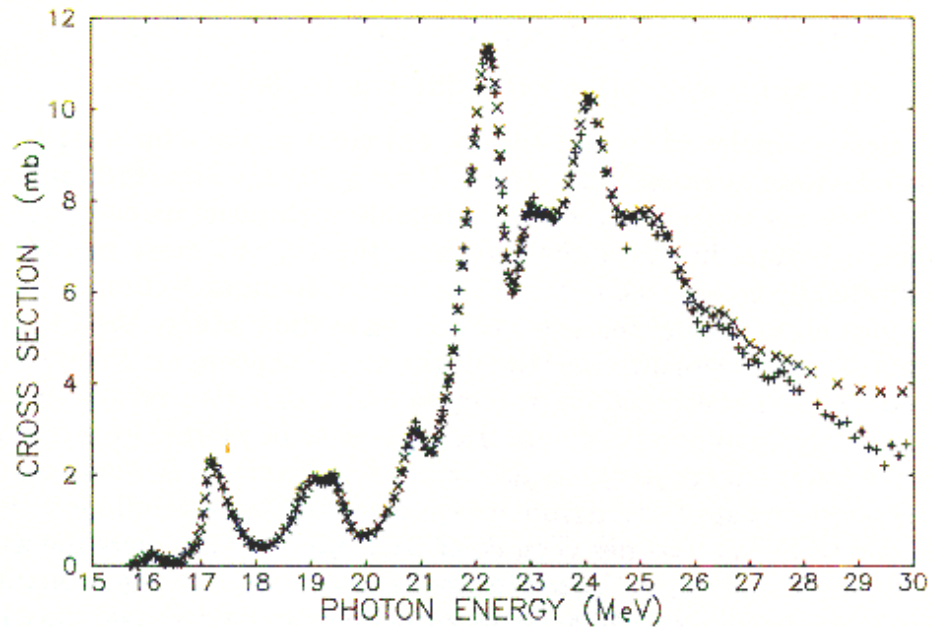
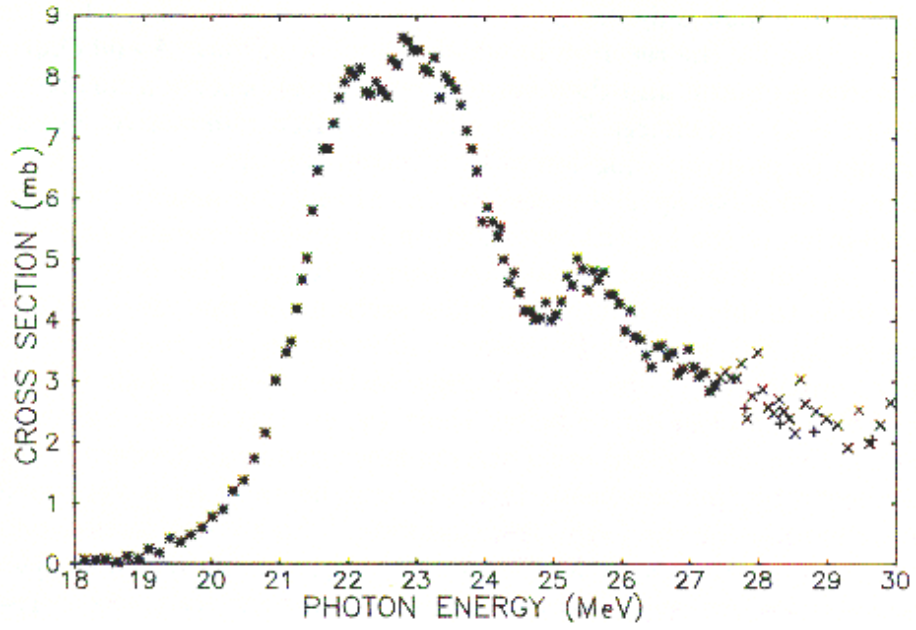


Figure 1-3. The (γ, xn) , represented as 'x', and (γ, n) , represented as '+', cross sections for ^{12}C (top) and ^{16}O (bottom). [NCR 84]

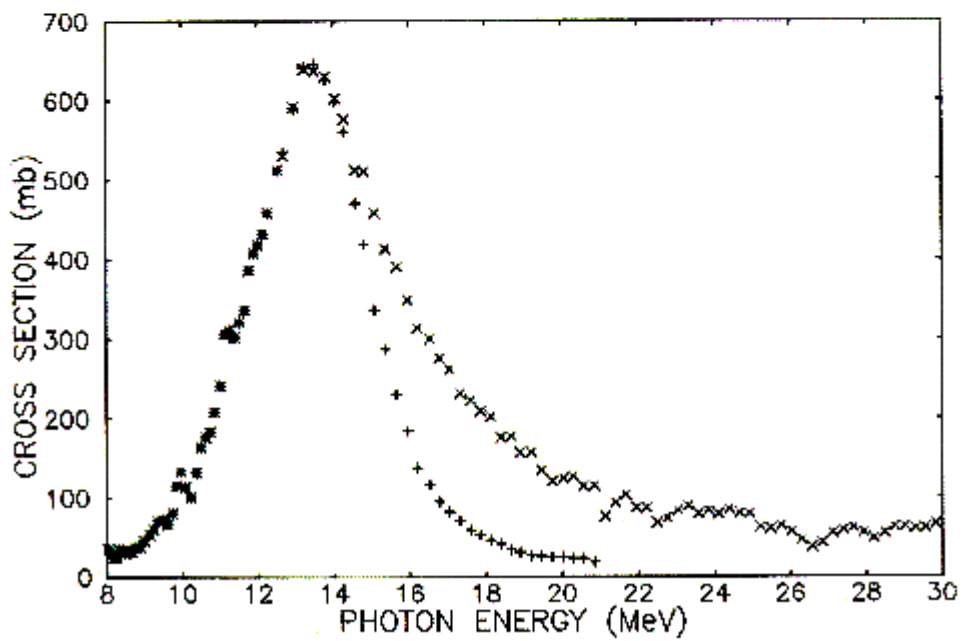
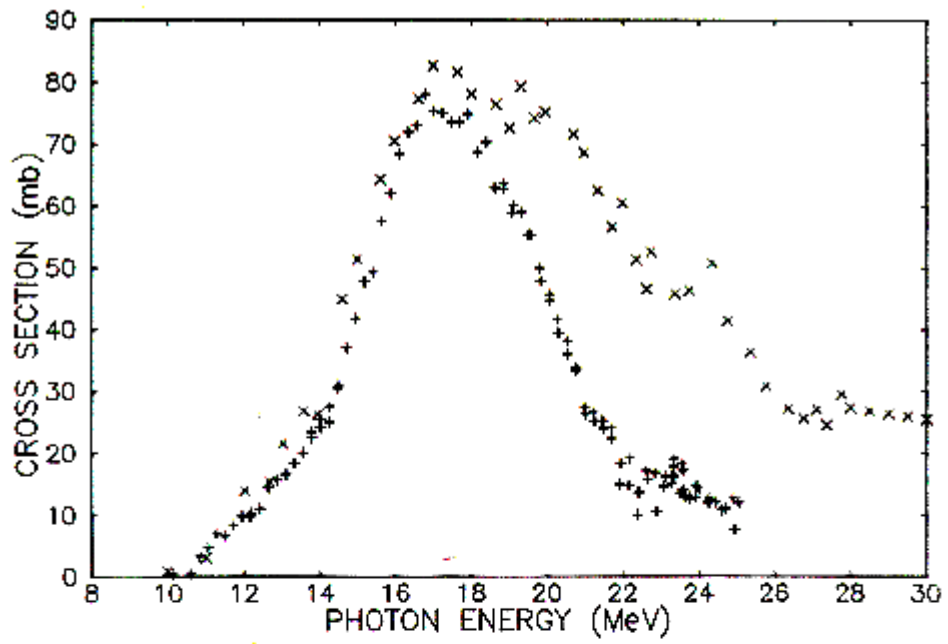


Figure 1-4. The (γ, xn) , represented as 'x', and (γ, n) , represented as '+', cross sections for copper (top) and ^{208}Pb (bottom). [NCR84]

Since the photons which initiate the photoneutron interactions come from the bremsstrahlung process, the ultimate neutron yield depends not only on the shape of the cross-section resonance curve, but also the shape of the bremsstrahlung spectrum generated by the electrons.

Figure 1-5 shows the neutron yield for different materials up to 40 MeV. A few materials requiring emphasis are those that form the target, which is usually an alloy. For instance, the Philips SL 75/5 linac has a 3mm-thick target composed of 95% tungsten, 3.75% nickel and 1.25% iron [LEW 99]. Figure 1-6 shows the relative neutron yield at different energies for a range of target thicknesses. Figure 1-7 and 1-8 show the photoneutron spectra from lead, carbon and oxygen.

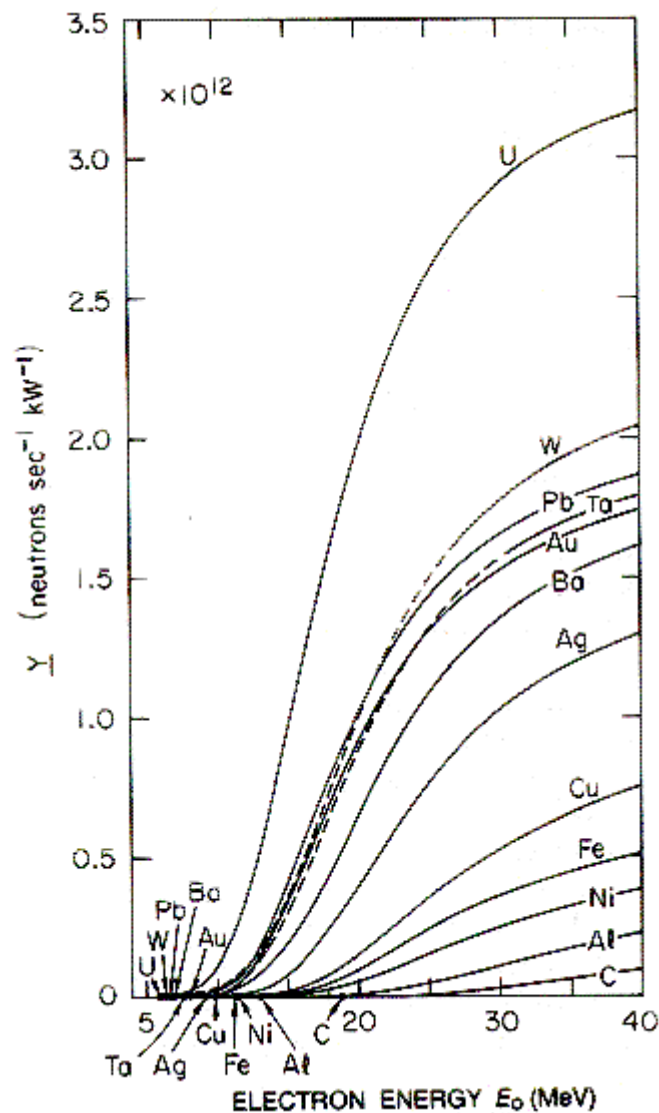


Figure 1-5. Thick target neutron yields. [SWA 79]

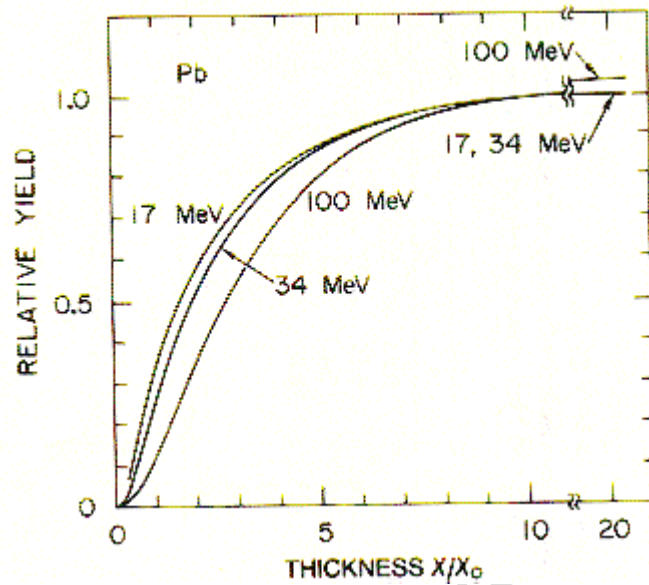


Figure 1-6. Relative neutron yield as a function of target thickness in radiation lengths X_0 . [SWA 78]

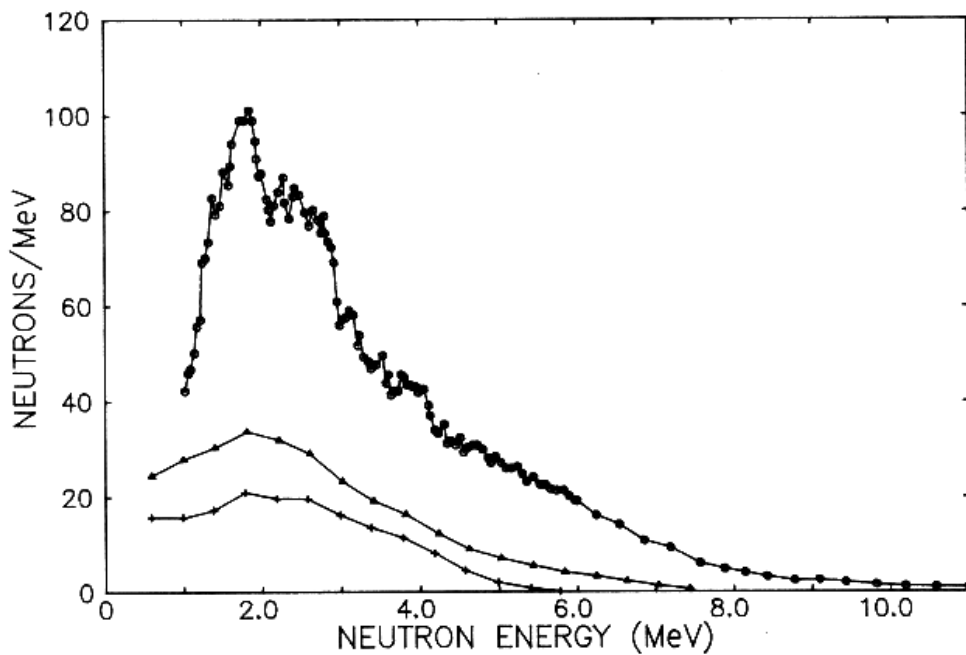


Figure 1-7. Photoneutron spectra from lead. Each of the 3 curves, starting from the top, is for 31, 15 and 13 MeV respectively. [NCR 84]

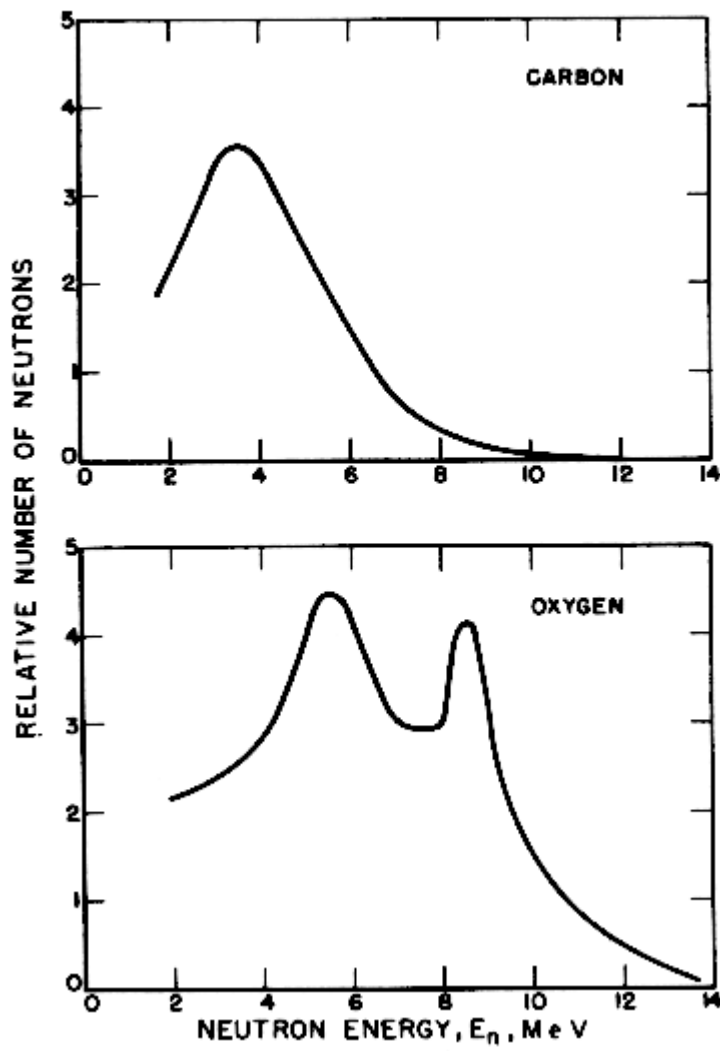


Figure 1-8 Photoneutron spectra from carbon and oxygen. [NBS 64]

downloaded from

1.1.org

Neutron Interactions

When neutrons or any neutron-induced radiation (eg. secondary photons) interact with tissues, energy is imparted to the tissues, causing biological hazard. The absorbed dose is the energy per unit mass imparted to the material by ionizing radiation. Depending upon the composition of the tissue, the interactions that occur between neutrons and tissue differ.

At epithermal energies, neutrons are moderated, i.e. slowed down, mainly by elastic scattering in hydrogen. Elastic scattering by hydrogen contributes up to 95% of the energy transferred by fast neutrons to tissue [NBS 64]. The elastic scattering process will be demonstrated using a C program in Chapter 3.

At higher energies, on the other hand, the predominant moderating effect comes from inelastic scattering in materials of high atomic number. This interaction does not occur at energies below the lowest excited state of the material. The lowest excited states for some isotopes are given in Table 1-4. It is difficult to quantify the energy loss due to inelastic scattering. More often than not, there will be a cascade of photon emissions and the relative yields need to be taken into account. It is only the minimum energy loss, which is equal to the energy of the lowest excited state, which can be readily quantified.

Table 1-4. First excited states.

ELEMENT	ATOMIC NUMBER	ABUNDANCE (%)	1 ST EXCITED STATE (MeV)
Pb	206	25.1	0.803
	207	21.7	0.570
	208	52.3	2.61
Fe	54	5.8	1.41
	56	91.7	0.847
W	182	26.4	0.100
	183	14.4	0.047
	184	30.6	0.111
	186	28.4	0.123

A third moderating process is the production of neutron pairs, i.e. the (n,2n) interaction which competes with inelastic scattering. Since the emerging neutrons have to share out the energy of the original neutron, each will have an energy lower than that of the parent neutron.

The capture process acts as a neutron sink, resulting in a decreasing number of neutrons. There are two types of capture: radiative capture and prompt disintegration. The important capture interactions in tissue are $^1\text{H}(n,\gamma)^2\text{D}$, which gives off a 2.2 MeV γ quantum, and $^{14}\text{N}(n,p)^{14}\text{C}$, which gives off a 600 keV proton.

Different interactions occur with different probabilities, which are energy and/or angle dependent. The probability of any interaction when a neutron passes through matter -- whether it is captured, elastically or inelastically captured -- is given by the corresponding neutron interaction cross-sections (expressed in barns).

Residual Activities

The unintended production of neutrons in the radiotherapy room leads to residual radioactivities. Both neutron emission and neutron capture are sources of residual radioactivities.

Neutron emission tends to yield isotopes that are neutron deficient and therefore unstable. Such isotopes may decay by giving off positrons, which in turn give off two 511 keV photons each. The degree of hazard depends not only on the abundance of the parent nuclide, but also on the half-life and the mode of decay of the daughter nuclide. In the event that the parent nuclide is low in abundance, the hazard is understandably lower.

The hazard is minimal if the half-life is extremely short (in which case the radioactivity dies off quick enough) or extremely long (in which case the decay rate is too slow to cause any harm). Neutron emission from aluminium, for instance, yields two isomeric forms, one of 6.7 seconds half-life and the other of 0.80 million years. As for the mode of decay, electron capture is not as much a cause for worry as positron emission.

Neutron capture requires separate discussions for fast neutrons and thermal neutrons. Capture of fast neutrons may result in particulate emissions, a special case being the multiplication of neutrons. Residual activity from capture of fast neutrons is generally insignificant, the worst case being the (n,α) reaction on

aluminium, producing ^{24}Na . For 1 g/cm^3 of aluminium, a 10^{13} per second fast-neutron flux would result in a saturation activity of 4mCi of ^{24}Na and a dose rate of 6 mSv/hr at one meter [NBS 64].

Capture of thermal neutrons takes place mainly in the concrete wall. The presence of sodium and manganese can be serious. If the concrete contains 1.6% of sodium by weight, 4.8% of neutron capture will then be in sodium, producing ^{24}Na which has a half-life of 15 hours [NBS 64]. Manganese, on the other hand, has a capture cross-section of 13 barns and produces ^{56}Mn , which has a half-life of 2.6 hours and decays by gamma emission of up to 3 MeV.

downloaded from www.marychm.org

Chapter 2. SHIELDING THE HAZARD

The presence of a hazard calls for protection. The room shielding material, usually concrete, protects the staff and the public over the other side of the wall or ceiling from the direct transmission of neutrons. The design of the maze, on the other hand, protects those near the room entrance, including staff working in the control room and those passing by.

The Material

Using tabulated data of neutron interaction cross sections at different energies [NBS 64], Figure 2-1 and Figure 2-2 are constructed. Figure 2-1 demonstrates the variation in neutron transmission as a function of energy, density and thickness. No monotonic trend can be observed from the neutron transmission as a function of energy because it depends on the neutron interaction cross sections.

Figure 2-2 compares the neutron shielding effects of various materials of thickness 1 m. Ordinary concrete and Barytes concrete are obviously more effective neutron shields than water and soil. Barytes concrete is markedly more effective than ordinary concrete at energies 8 to 10 MeV. Water acts as a better neutron shield than earth because of its hydrogen content.

Additional shielding of neutrons can be achieved by having a door at the entrance of the room. This is, however, not recommended since it complicates patient transport. Worse still, the patient may be trapped inside when the door fails.

Special care must be taken not to forget about neutron shielding when planning to shield against photons. As mentioned earlier, high density materials such as metals can be excellent photon shields but also terrible sources of neutrons. It has been found that a lead wall gives a higher neutron dose equivalent of 23 mSv per Gray x-ray dose [McG 92]. A good way of shielding against neutrons would be to laminate neutron-moderating materials in the concrete walls. The shielding effects of some moderating materials are compiled in Table 2-1 based on a study to quantify the effect [LAL 97].

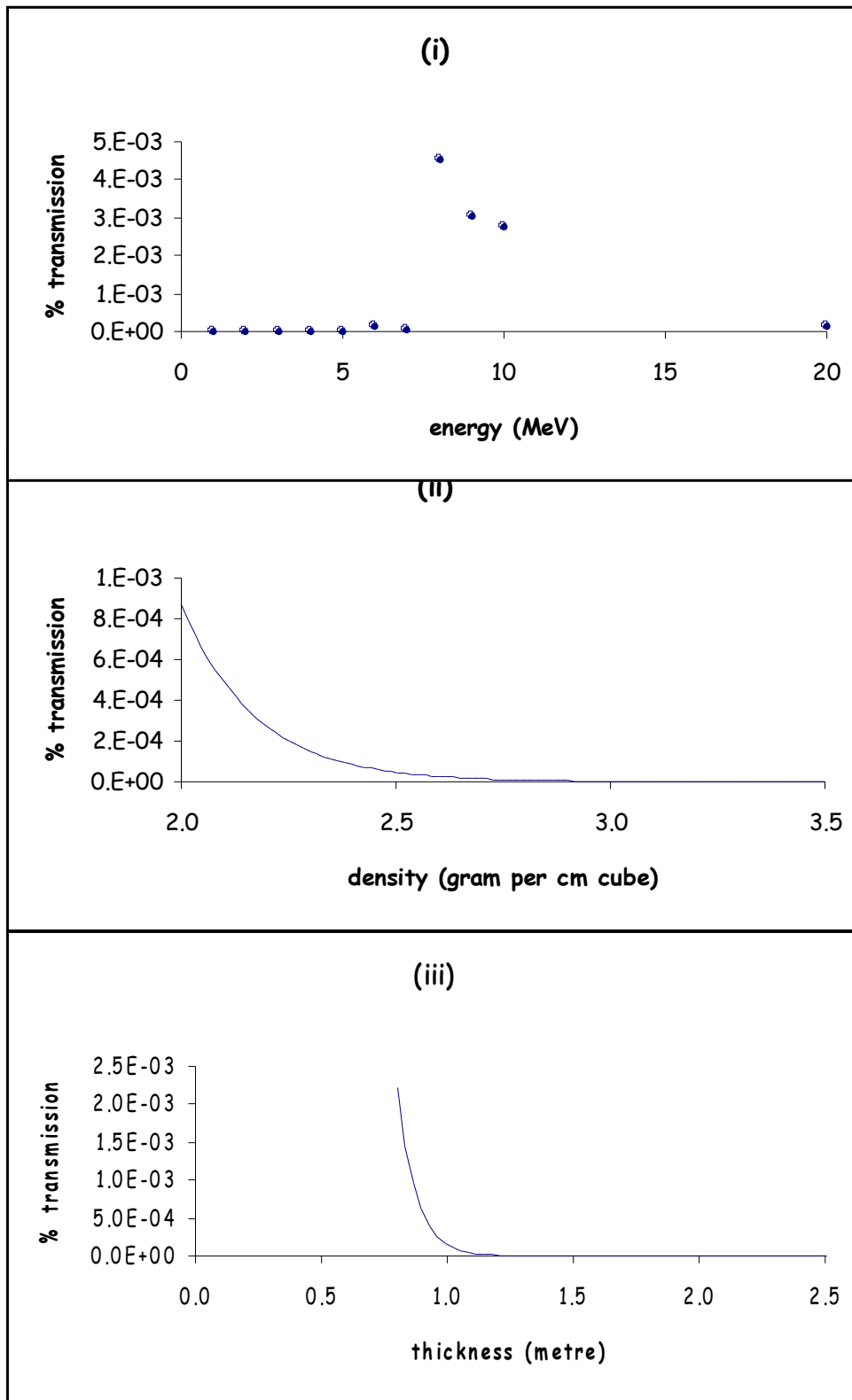


Figure 2-1. Neutron transmission for ordinary concrete as a function of
 (i) neutron energy, density = 2.3 g/cm³, thickness = 1 m,
 (ii) density of shielding material, thickness = 1 m, energy = 20 MeV and
 (iii) thickness of shielding material, density = 2.3 g/cm³, energy = 20 MeV.

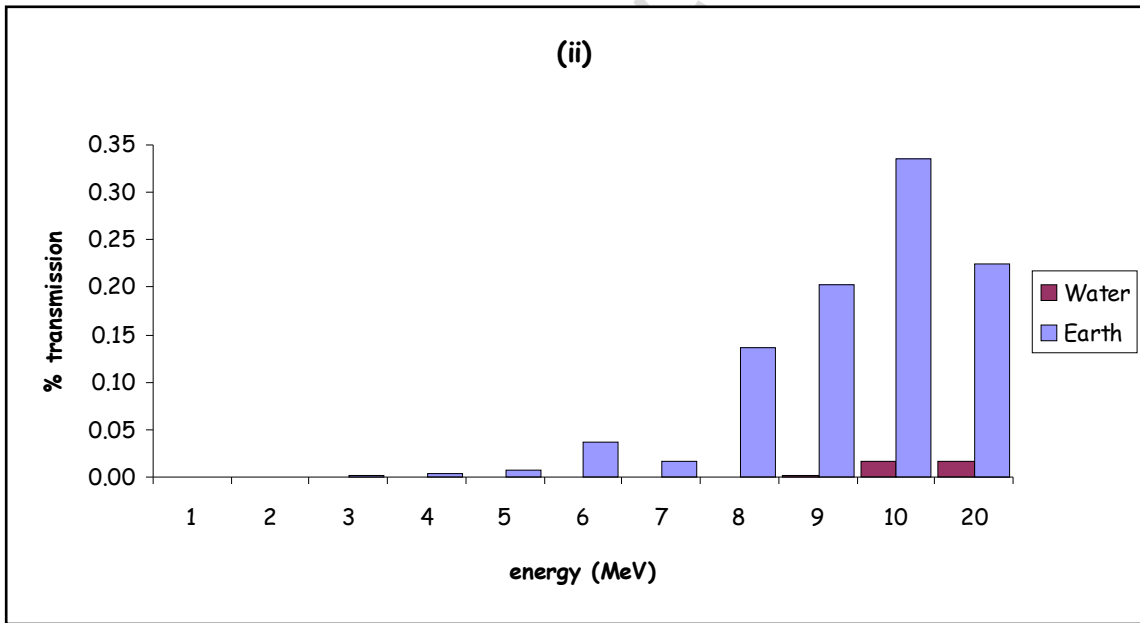
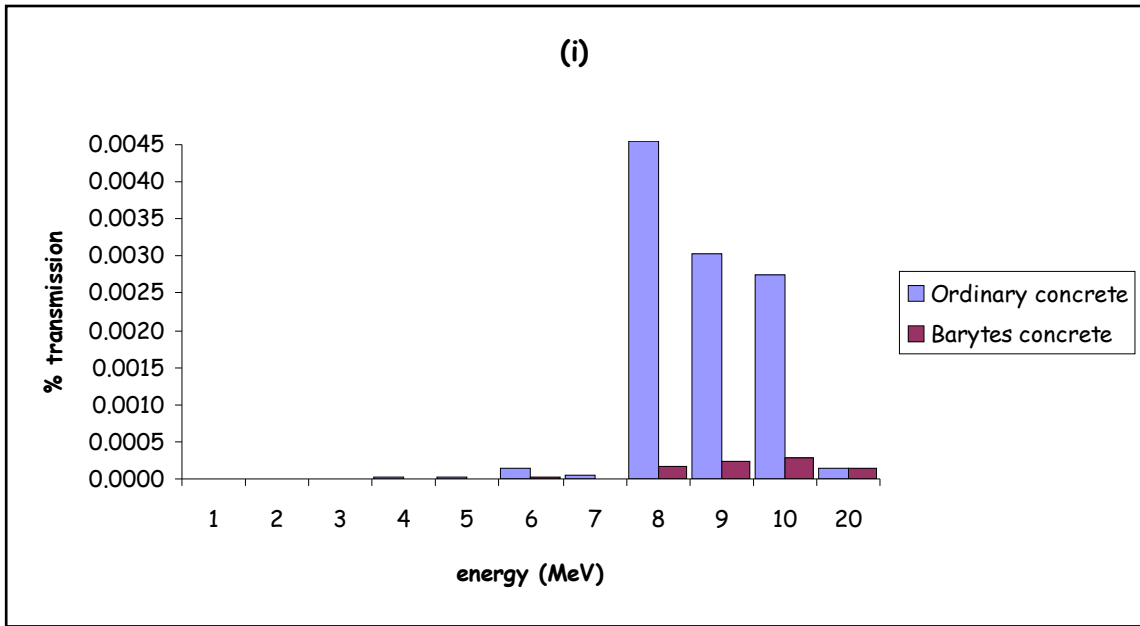


Figure 2-2. Neutron transmission of different shielding materials, thickness = 1 m:
 (i) ordinary concrete, density = 2.3 g/cm^3 and Barytes concrete, density = 3.1 g/cm^3 ,
 (ii) water, density = 1.0 g/cm^3 and earth, density = 1.0 g/cm^3 .

Table 2-1. Shielding effects of neutron-moderating materials.

MAZE LINING	REDUCTION IN NEUTRON DOSE	REDUCTION IN PHOTON DOSE
Polyethylene	27%	Not much
Polyethylene + flexboron	50%	32%
Polyethylene + boron In maze doors	92%	55%

The Design

In terms of neutrons a basic requirement for the design of a radiotherapy maze is to avoid first-scatter neutrons at the entrance of the maze. That is, neutrons arriving at the entrance of the maze should have been scattered at least twice. Figure 2-3 illustrates this. Apart from that, a double-bend maze shields neutrons better than a single-bend maze and is therefore recommended where possible.

The requirement on barrier thickness is greater for regions of the wall where the primary photon beam from the treatment head strikes. This is shown as bulges of concrete in Figure 2-3. While neutrons are isotropic, photons are not - they depend on the gantry angle. This is therefore a shielding requirement for photons, not neutrons. The pieces of extra thickness, either bulging in or out, are required to take into account the possible gantry angles. The extra pieces on walls N and S account for gantry angles 90° and 270° respectively. Another extra piece over the ceiling accounts for gantry angle 180°. Since installations are normally done on the ground floor, gantry angle 0° is allowed to radiate directly into the soil with less worry.

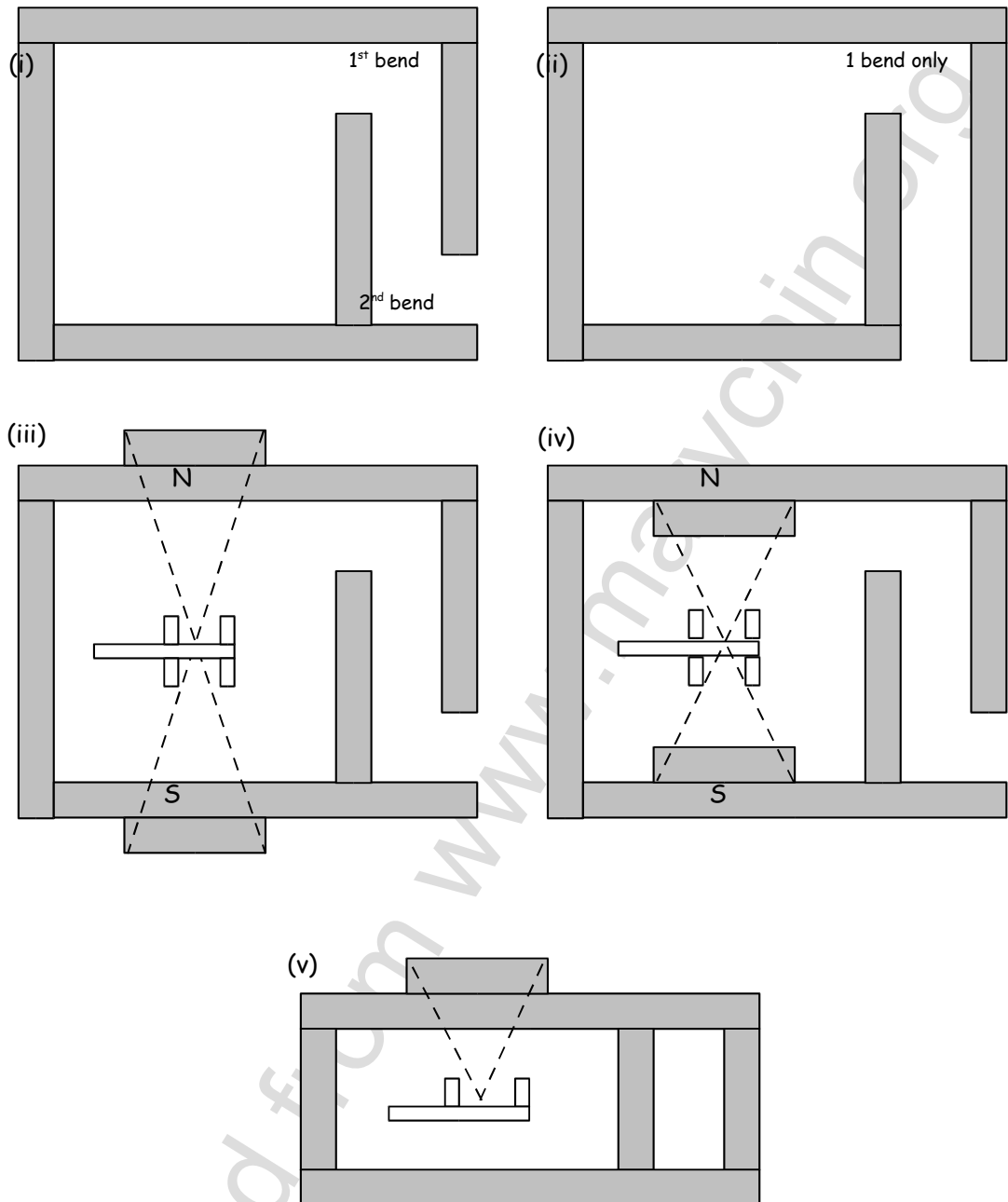


Figure 2-3. Maze designs. (i) a double-bended maze which offers better neutron attenuation than (ii) a single-bended one. (iii) and (iv) shows extra pieces of concrete on two of the walls to account for the primary photon beams at gantry angles 90° and 270°. (v) shows the extra piece over the ceiling top to account for primary photon beams at gantry angle 180°. The gantry and the edges of the primary beams are shown.

Chapter 3. QUANTIFYING THE HAZARD I: THE APPROACH

Deterministic Approach

The deterministic approach uses formulae to quantify particle transport. The method is straight-forward: demanding no sophisticated computing facility, no long waiting time for sampling particle histories, and requiring no generation of random numbers.

A simulation is a realisation, with the best possible accuracy, of the behaviour of the particles. The following is an example of a deterministic simulation. It is based on a C program written by the author that simulates neutron moderation by elastic scattering.

A Deterministic Simulation

When photons produced in a medical linac impinge on the various parts in the accelerator head, the patient and the walls of the bunker, the (γ, n) reaction, i.e. photodisintegration, takes place. The photoneutrons emitted are mainly moderated by elastic scattering between the neutrons and the target elements although there are some other processes which may contribute as mentioned in Chapter 1.

In an elastic collision between a neutron and a target atom initially at rest, applications of the laws of conservation of energy and linear momentum leads to:

$$\begin{aligned} E &= \text{initial neutron energy in the laboratory system} \\ E' &= \text{final neutron energy in the laboratory system} \\ A &= \text{mass of target atom} \\ \theta &= \text{scattering angle in the centre-of-mass system} \end{aligned} \quad \frac{E'}{E} = \frac{A^2 + 2A \cos\theta + 1}{(A+1)^2} \dots\dots\dots(1)$$

This ratio is minimum for the case of a head-on collision:

$$\left(\frac{E'}{E}\right)_{\min} = \left(\frac{A-1}{A+1}\right)^2 \dots\dots\dots(2)$$

If parameter ξ represents the average value of $\log(E'/E)$ after a single collision and n the number of collisions,

$$\xi = 1 + \frac{(A-1)^2}{2A} \ln \frac{A-1}{A+1} \dots\dots\dots(3)$$

$$\ln E' = \ln E - n\xi \dots\dots\dots(4)$$

[KRA 88]

Based on the above relations, the following table is constructed:

Table 3-1. Calculation for elastic collisions.

NUCLIDE CONSIDERED*	$\left(\frac{E'}{E}\right)_{\min}$	ξ	NO. OF GENERATIONS TO REACH THERMALISATION		
			$E_{\gamma}=5\text{MeV}$	$E_{\gamma}=10\text{MeV}$	$E_{\gamma}=20\text{MeV}$
^1H	0.000	1.000	19	20	21
^{16}O	0.779	0.120	123	127	131
^{12}C	0.716	0.158	142	147	152
^{14}N	0.751	0.136	161	167	173
^{27}Al	0.862	0.072	268	277	287
^{184}W	0.978	0.011	1785	1849	1913
^{208}Pb	0.981	0.010	2017	2090	2162

*In patient: ^1H , ^{16}O , ^{12}C and ^{14}N . In air: ^{16}O and ^{14}N .

In accelerator head and accessories: ^{184}W , ^{208}Pb and ^{27}Al .

To illustrate the effects of elastic scattering on the neutron spectrum, a computer program is written to track subsequent generations of collisions until the average energy reaches 0.025 eV. For a target of ^1H and an initial monoenergetic energy of 20 MeV, 21 generations are required for thermalisation. The spectra for the first three, the fourth and the last are shown in Figure 3-1. Those in between have a similar shape as the fourth, but with an increasing population shift to the lower energies.

A point to note is that the area under each spectrum is constant throughout all generations. The total number of neutrons, 10000, is constant throughout all generations since this example assumes no absorption. 10000 are sufficient for this simulation since it is deterministic -- a Monte Carlo simulation would require more. As the spectrum progresses through subsequent generations, more and more neutrons have lower and lower energies, and, consequently, less and less neutrons have high energies.

The higher the initial energy the higher the number of collisions are required in order to reach thermalisation. Variations caused by different initial energy and different target nuclei are given in Table 3-1.

For a less efficient moderator, the spectrum takes many more generations of collisions to reach an average thermal energy. Its shape can be remarkably

different for the earlier generations, showing a bell shape with a peak. This bell shape slowly evolves into the $1/E$ shape as the spectrum progresses through the generations. The spectra for lead as the moderator are shown as an example in Figure 3-2 and Figure 3-3, where it takes 2090 generations to be thermalised.

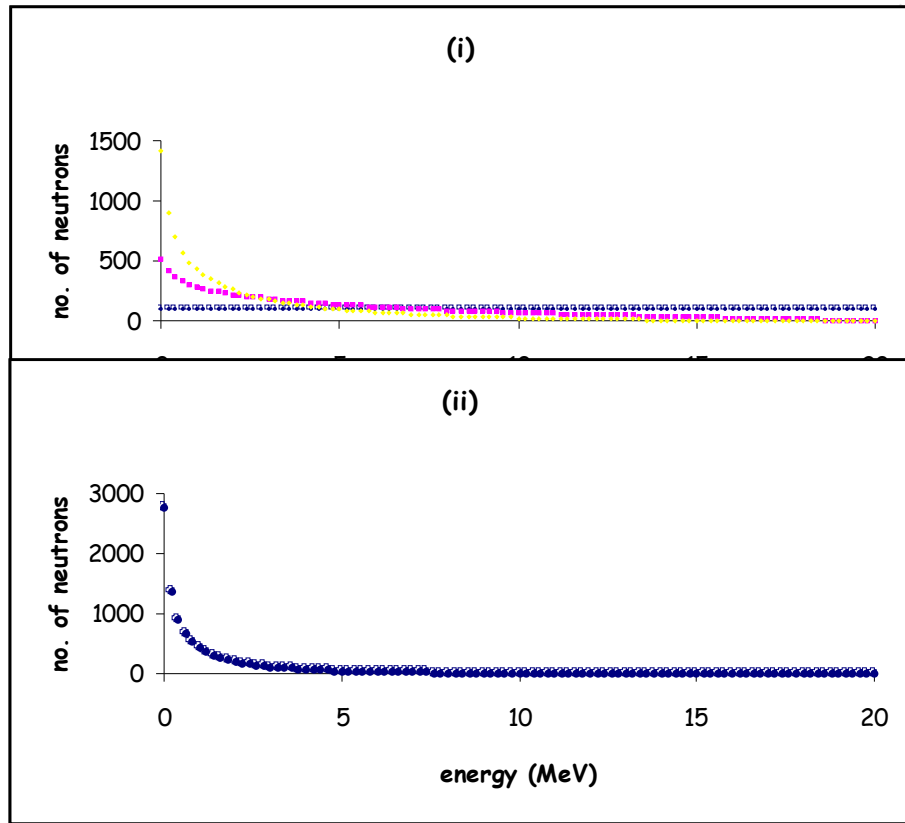
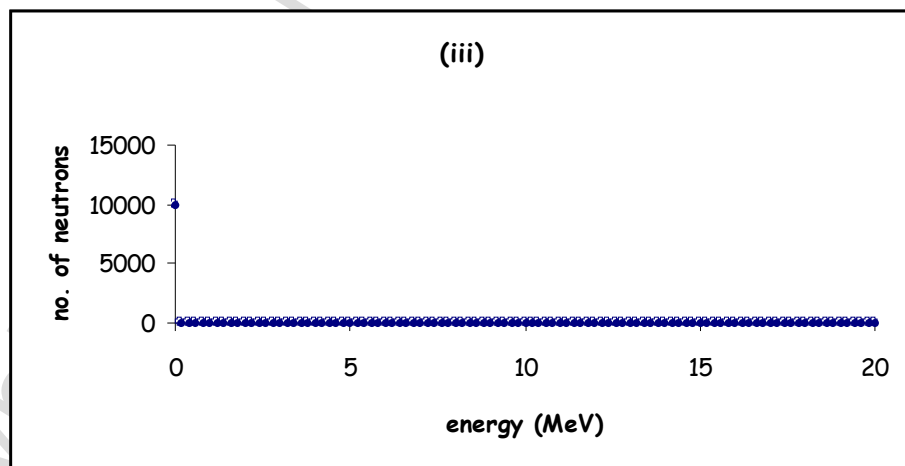


Figure 3-1. Neutron spectra through generations of elastic scattering.
Moderator: ^1H . Initial Energy = 20MeV.

(i) The first three generations. (ii) The fourth generation.



(iii) The 21st generation, the last.

How each spectrum is built: a step-by-step example

Figure 3-2. Neutron spectra through generations of elastic scattering by Pb-208:
The first 50 generations.

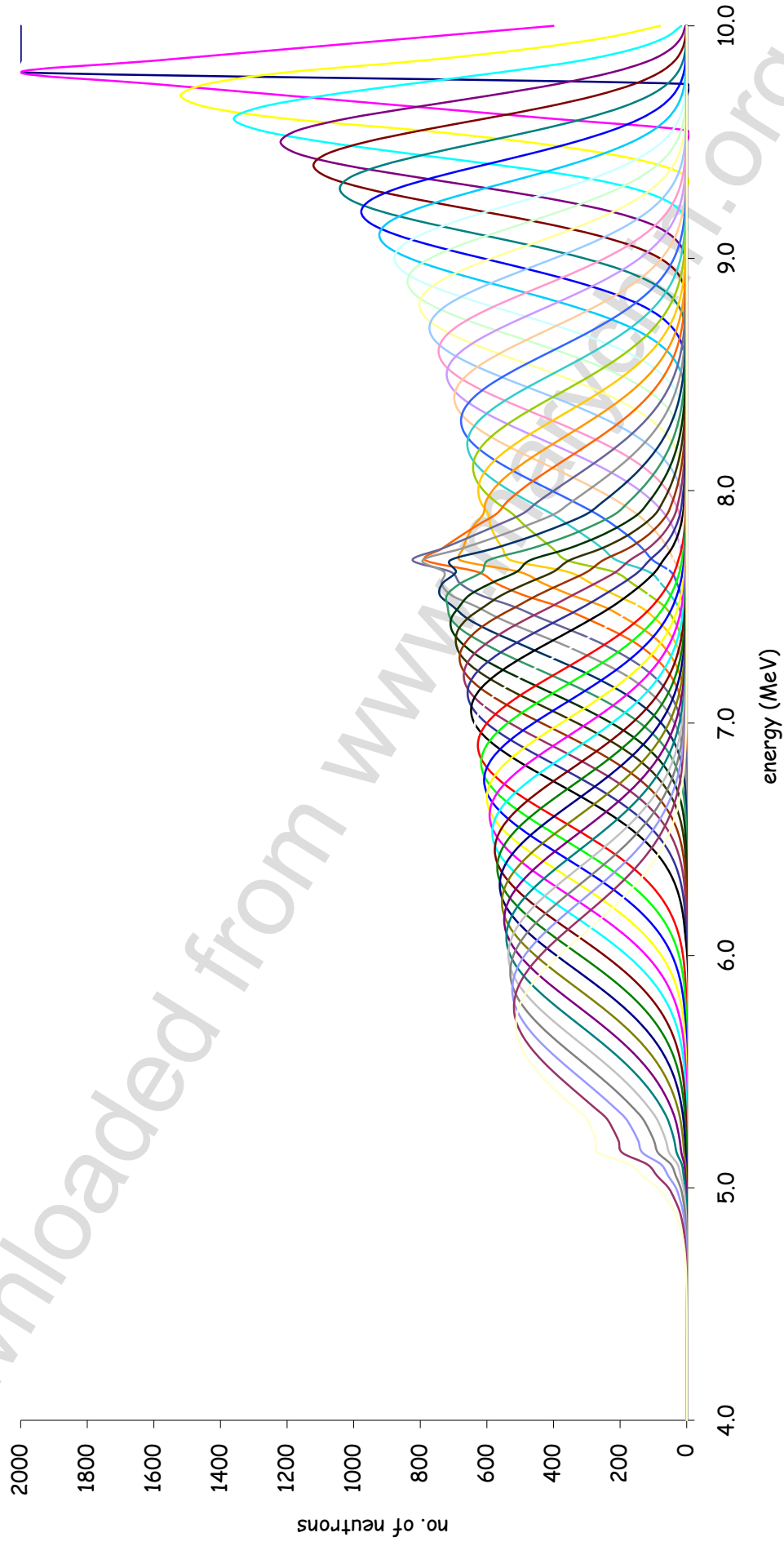
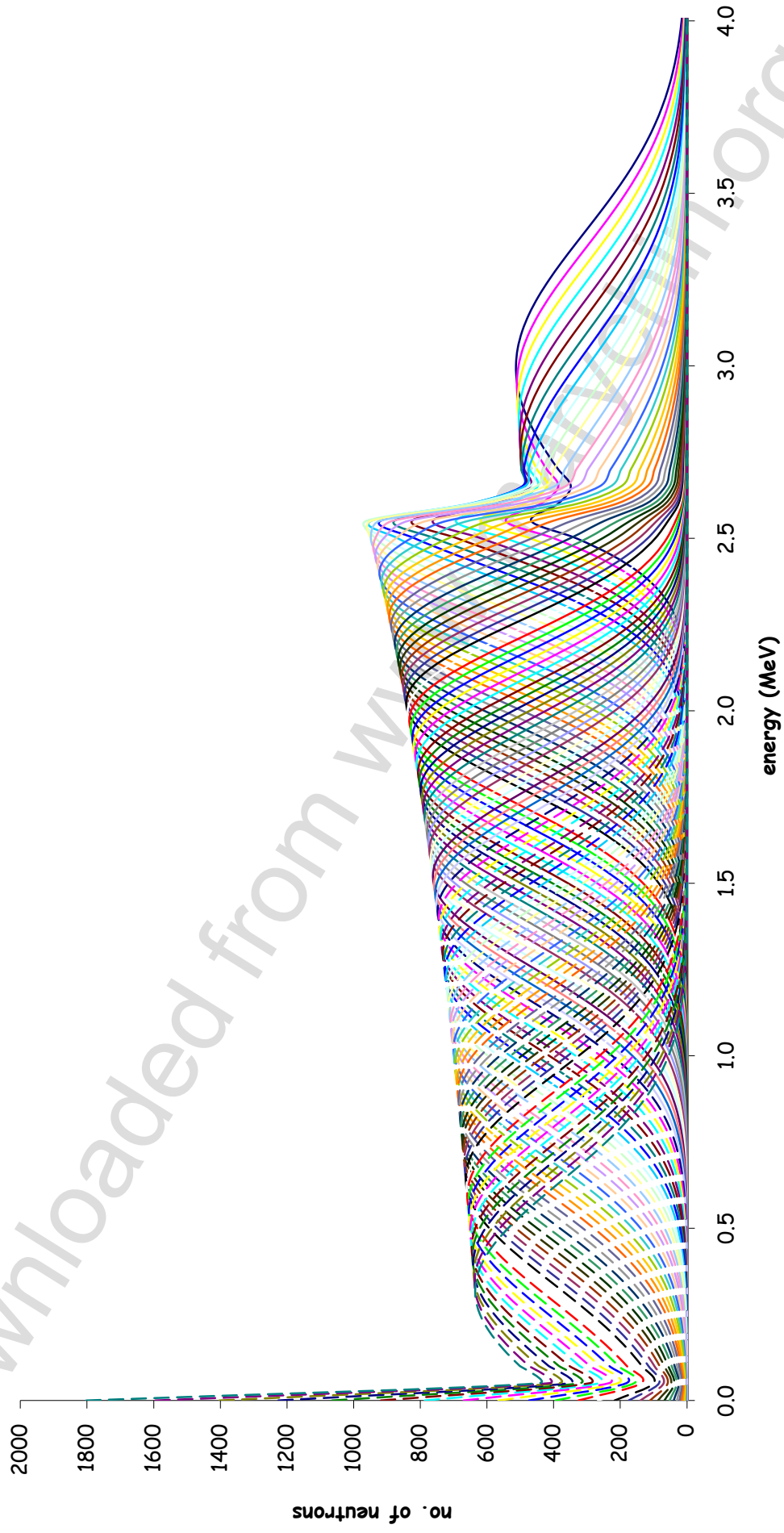
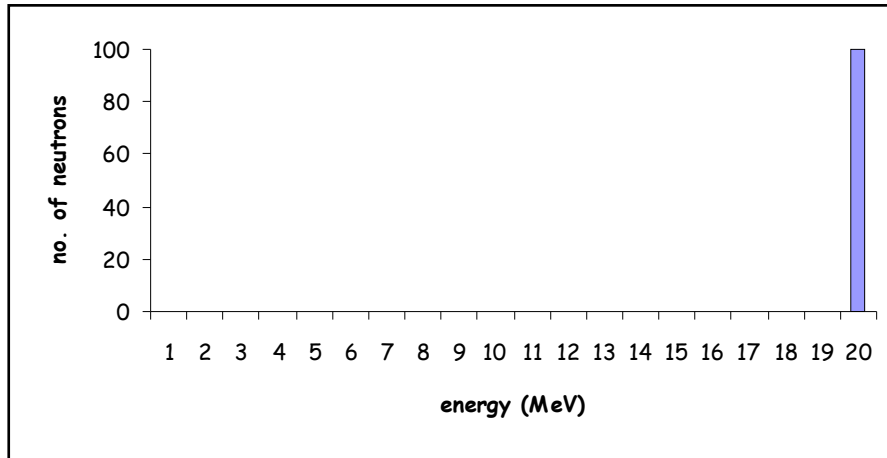


Figure 3-3. Neutron spectra through generations of elastic scattering by Pb-208: the 101th to the 200th generation.



Incident generation: Consider the case of ^{12}C . Start with a monoenergetic beam: $E = 20$, initial number of neutrons $N = 100$.

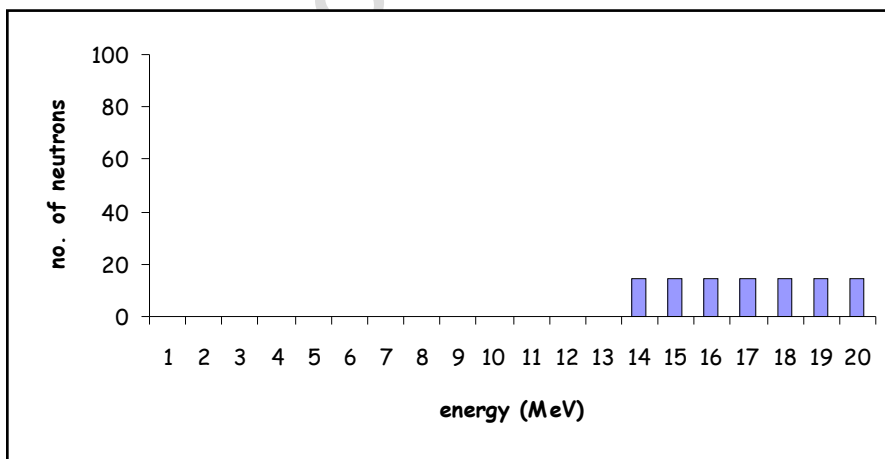


1st generation: Find the left leg, i.e. the new minimum energy for this generation, using Eq (2):

$$E = 20 \quad \left(\frac{A-1}{A+1} \right)^2 = 0.7 \quad \therefore E'_{\min} = 20 \times 0.7 = 14$$

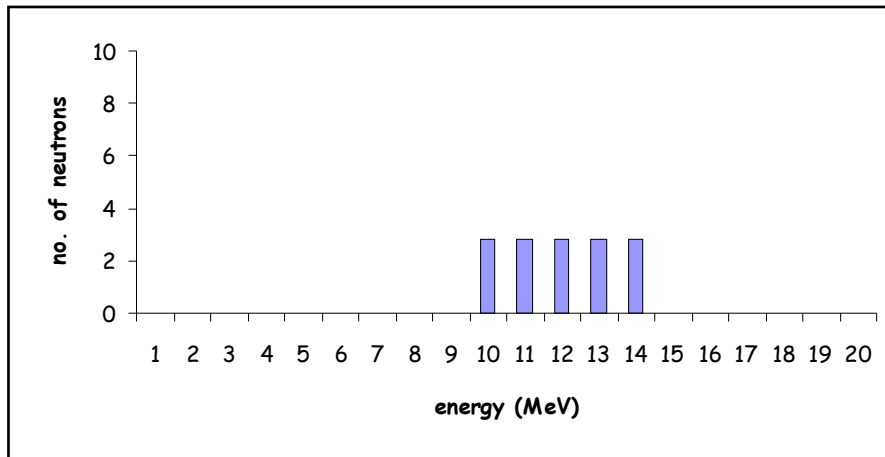
Find the new height so that the initial number of neutrons is evenly distributed across the new energy range:

$$N' = \frac{100}{20 - 14 + 1} = 14.3$$

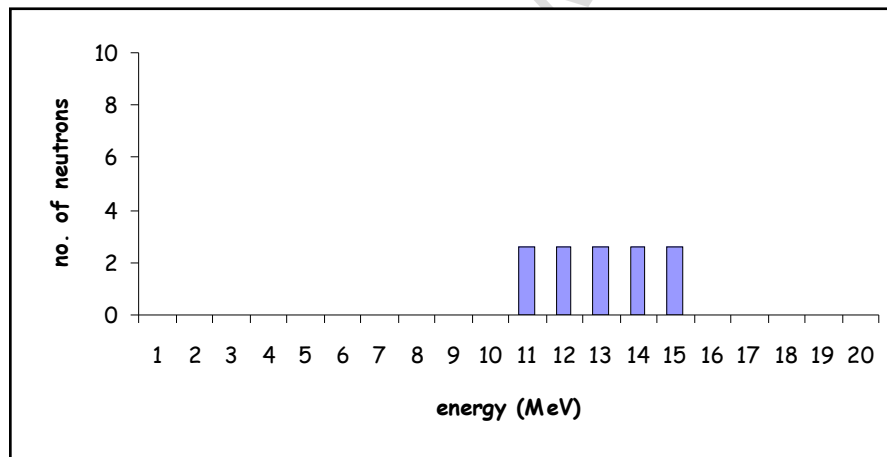


2nd generation: Take $E = 14$, find the new left leg and the new height:

$$E = 14 \quad E'_{\min} = 14 \times 0.7 = 9.8 \quad N' = \frac{14.3}{14 - 9.8 + 1} = 2.8$$

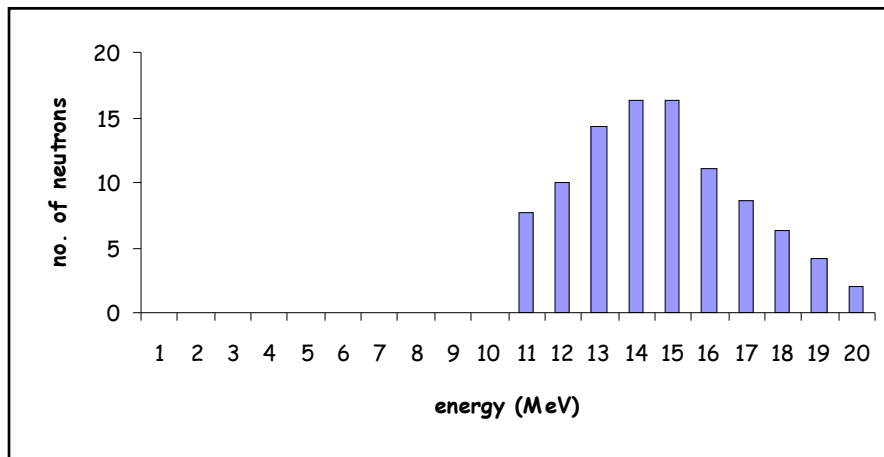


Repeat the same for $E = 15$: $E'_{\min} = 10.5$, $N' = 2.6$



Repeat the same for $E = 16, 17, 18, 19$ and 20 . We get a total of 7 distributions of rectangular shape as shown for $E = 14$ and $E = 15$. Sum these 7 distributions together to obtain the spectrum for the second generation:

downloaded



3rd generation: Take E = 10, 11, 12, ..., 20, build distributions of rectangular shape for each and sum them all together to obtain the spectrum for the third generation... and so forth to build the subsequent spectra.

It is based on this algorithm that the program is written, which produces the data for spectra shown in Figures 3-1, 3-2 and 3-3. This program is then taken a step further to moderate neutrons from a ²⁵²Cf fission source, instead of monoenergetic neutrons. Of interest here are neutrons produced in the case of a medical linac, where the primary neutrons were found to approximate a ²⁵²Cf fission spectrum. The ²⁵²Cf fission spectrum is generated using the equation:

$$\frac{dN}{dE} = \sqrt{E} e^{-E/1.3} \dots\dots(5)$$

[KNO 79]

where E is the energy in MeV. The spectra are shown in Figure 3-4.

downloaded from www.indjournals.org

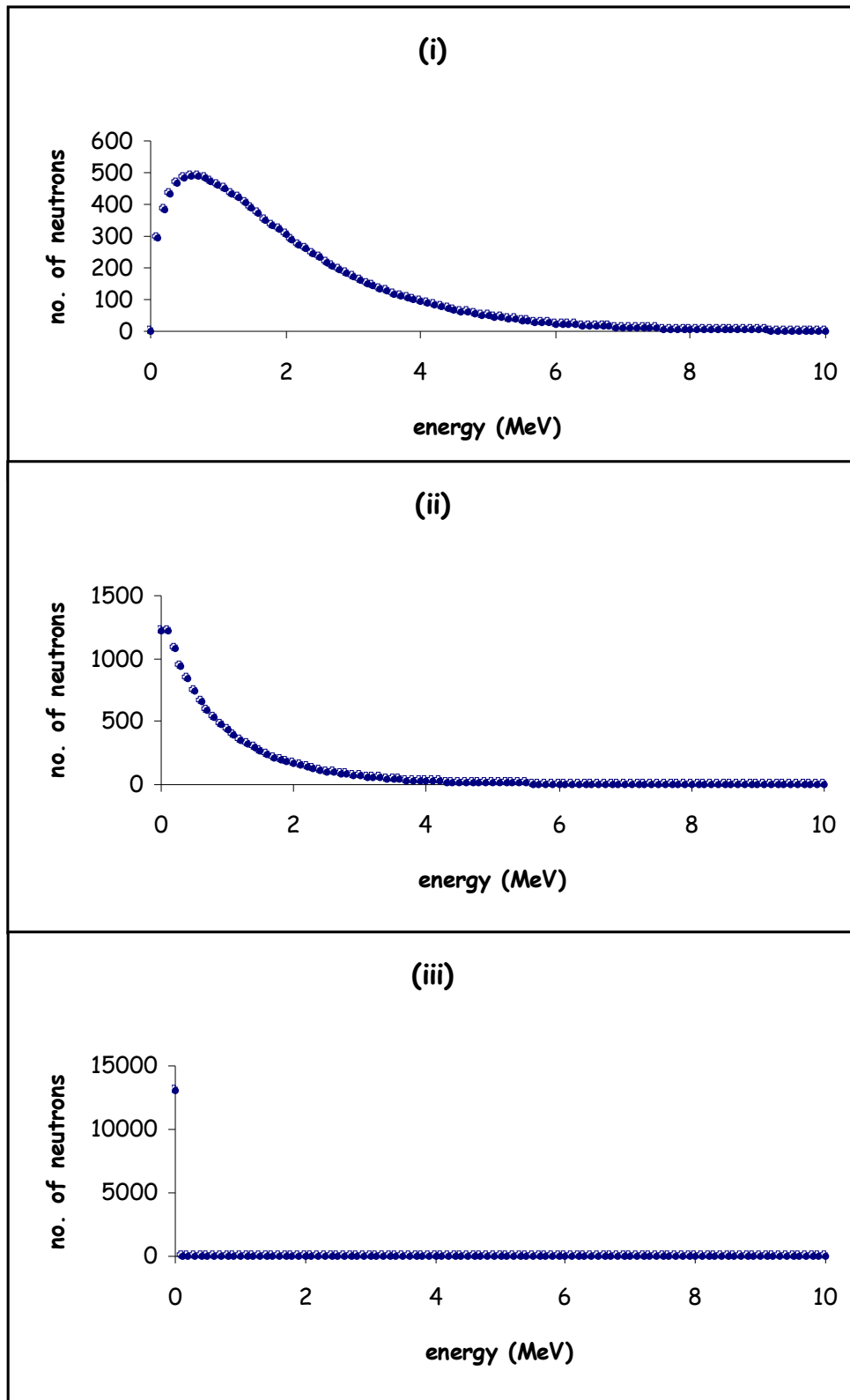


Figure 3-4. Neutron spectra. Moderator: ^1H . (i) initial ^{252}Cf fission source (ii) after 1 generation of elastic collisions. (iii) after 18 generations of elastic collisions.

Monte Carlo Approach

The Monte Carlo approach is based on random sampling. While the deterministic approach sets out to produce the value of a desired physical quantity, the Monte Carlo approach produces the expected value of a random variable.

A simulation is a mimic of the actual, physical process. Simulations may be analog or non-analog. The analog model uses natural probabilities that various events occur. While analog Monte Carlo simulates the real physical events directly, non-analog Monte Carlo deviates from any strict one-to-one simulation of the actual physical process. The reason to go for a non-analog simulation is to save computing time - which can be far from reasonable if every single particle is to be faithfully followed throughout its entire history. Starting with less source particles does help in reducing computing time but does not help the problem as a whole since it only leads to results of lower confidence. Results obtained from a good non-analog simulation should converge with those from an analog simulation.

The story of a particle's life is about randomness. From the very beginning, its emission from the source is random, its initial energy (if there is an energy distribution), initial direction and initial location (if the dimensions of the source is finite) are all random. During its transport, where and when it interacts are random. The type of interaction is also random - whether it is captured, elastically or inelastically scattered. If scatter occurs, the energy loss and the angular deviation are random (hence the term 'random walk'.) If a multiplicative interaction occurs, the number of daughters produced is random. As one tries to detect the particle, whether the particle enters the space of detection interest and whether it interacts in a suitably detectable manner are random.

To describe the total phenomenon, a Monte Carlo simulation samples statistically the probabilistic distributions governing the individual probabilistic events. The life history of a particle spans from its emission to its termination. It terminates when it is absorbed or when it leaves the system and never comes back. If variance reduction techniques are introduced, still more ways can be adopted to terminate it.

MCNP

In this work, MCNP -- a general Monte Carlo N-Particle Transport Code version 4B, is used for to simulate a radiotherapy maze. It is developed by the Transport Methods Group of Los Alamos National Laboratory. Some existing Monte Carlo codes are given in Table 3-2.

Table 3-2. Some existing Monte Carlo codes.

CODE	ESTABLISHMENT
APM	Lawrence Livermore National Laboratory (LLNL, USA)
EGS	Stanford Linear Accelerator Center (SLAC, USA) National Laboratory for High-Energy Physics (KEK, Japan) National Research Council of Canada (NRCC, Canada)
ETRAN	National Institute of Standards and Technology (NIST, USA; formerly National Bureau of Standards, NBS)
ITS	Sandia National Laboratories (SAND, USA)
MCEF	University of Zaragoza, Spain Karolinska Institute-University of Stockholm, Sweden
MCNP	Los Alamos Scientific Laboratory (LASL, USA)
MOCA	Gesellschaft für Strahlen- und Umweltforschung (GSF, Germany)
MORSE	Oak Ridge National Laboratory (ORNL, USA)
OGRE	Oak Ridge National Laboratory (ORNL, USA)
OREC	Oak Ridge National Laboratory (ORNL, USA)

MCNP simulations do more than just generating random numbers through the random walks and extracting appropriate values from the cross sections library. It also simulates in great detail the effects of thermal motion and chemical binding.

A brief overview of the MCNP will be presented here, with direct reference to the model simulated in this work.

The simulation process starts with an input file and ends with an output file. Both are text files. The input file is supplied by the user and the output file is generated

by the MCNP. The former gives the instructions by specifying the problem to be solved and the tallies expected by the user. A tally is the quantity of interest requested by the user. It is the information the user wishes to obtain from the simulation. The output file is usually very large, filled with abbreviations and numbers, which requires considerable skills to interpret.

The code, i.e. the input file, consists of geometry, source, material and tally specifications, along with the mode and the problem cutoff procedure. All simulations are done in neutron mode except the one for tallying secondary photons which is done in neutron-photon mode. The difference is: the neutron-only mode does not follow any photons produced. The simulation of the various interactions is the point in a Monte Carlo simulation where the procedures applied in neutron and photon transport calculations differ. The techniques for neutrons are more challenging because there is a greater variety of important interactions and the cross-section dependence on energy is less smooth. [LUX 91]

The problem cutoff is set to a time limit for most cases, instead of a number-of-histories limit. This gives more control over the simulation time. After the elapse of the time limit, if the number of histories is found to be insufficient, the run can then be continued from where the histories last terminated.

The geometry is specified in the cell cards and the surface cards. A card is simply an input line of maximum 80 columns. The input file is made up of such cards. In the simulations done in this work, each required different tally specifications, variance reduction techniques, and sometimes even modifications to the geometry. Therefore, the codes are different for each simulation. Only a simplified version will be presented here as an example. It tallies for the neutron dose equivalent at the entrance of the maze. The concrete walls, in this case, are not sliced into different cells as done in the actual simulation.

The cell cards used are:

```

1   0 1:-23:24                               IMP:N 0
2   1 -2.43 2 -3 11 -14 19 -20               IMP:N 1
3   1 -2.43 4 -5 12 -17 19 -20               IMP:N 2
4   1 -2.43 6 -7 16 -14 19 -20               IMP:N 2
5   1 -2.43 11 -12 3 -7 19 -20              IMP:N 2
6   1 -2.43 13 -14 3 -6 19 -20              IMP:N 1
7   1 -2.43 8 -9 10 -11 18 -21              IMP:N 1
8   1 -2.43 8 -9 14 -15 18 -21              IMP:N 1
9   2 -1.225E-3 3 -4 12 -13 19 -20 27       IMP:N 1
10  2 -1.225E-3 4 -5 17 -13 19 -20          IMP:N 2
11  2 -1.225E-3 5 -6 16 -13 19 -20          IMP:N 2
12  2 -1.225E-3 5 -29 12 -16 19 -20 #21     IMP:N 2
13  3 -1.25 -18 23 -1                         IMP:N 1
14  1 -2.43 18 -19 2 -7 11 -14              IMP:N 2
15  1 -2.43 20 -21 2 -7 11 -14              IMP:N 2
16  1 -2.43 21 -22 8 -9 10 -15              IMP:N 1
17  2 -1.225E-3 #1 #2 #3 #4 #5 #6 #7 #8 #9 #10 #11 #12 #13 #14 #15 #16 &
    #18 #19 #20 #21                           IMP:N 1
18  2 -1.225e-3 19 -20 -25                  IMP:N 1
19  2 -1.225e-3 19 -20 25 -26              IMP:N 1
20  2 -1.225e-3 19 -20 26 -27              IMP:N 1
21  2 -1.225E-3 -28                         IMP:N 2 FCL:N 1

```

The cell importances are specified at the end of each cell specification. 21 cells are specified here. The first, a void cell, defines the boundary beyond which particles are not to be followed. It is illegal not to have this boundary defined. The reason is obvious: particles cannot be followed to the infinite eternity. The other cells define the concrete walls and air spaces in and outside the room. In MCNP, cells are defined according to surfaces, not to coordinates. This is handy since any changes to the coordinates and dimensions can be made universally for all cells by changing the surface cards, listed below:

```

1   SY 150 900
2   PY -500
3   PY -400
4   PY 400
5   PY 500
6   PY 700
7   PY 800
8   PY -200
9   PY 200
10  PX -600
11  PX -500
12  PX -400
13  PX 400
14  PX 500
15  PX 600
16  PX -200
17  PX 200
18  PZ -170
19  PZ -150
20  PZ 150
21  PZ 250
22  PZ 350
23  PZ -370
24  PZ 550
25  CZ 100
26  CZ 200
27  CZ 300
28  S -300 800 0 10
29  PY 900

```

These surfaces are the boundaries of the cells defined earlier. In this case, most are planes, with a few spheres and cylinders. The surface cards are then followed by the data cards:

```

SDEF ERG=D1
SP1 -2 1.2895
F24:N 21
F34:N 21
DD 0.5
DXT:N -300 800 0 11 11
DE24 2.5e-8 1e-7 1e-6 1e-5 1e-4 1e-3 1e-2 1e-1 5e-1 1 2.5 5 7 10 14 20
DF24 3.67e-6 3.67e-6 4.46e-6 4.54e-6 4.18e-6 3.76e-6 3.56e-6 2.17e-5 &
      9.26e-5 1.32e-4 1.25e-4 1.56e-4 1.47e-4 1.47e-4 2.08e-4 2.27e-4
DE34 2.5e-8 1e-7 1e-6 1e-5 1e-4 1e-3 1e-2 1e-1 5e-1 1 2 5 10 20
DF34 3.85e-6 4.17e-6 4.55e-6 4.35e-6 4.17e-6 3.7e-6 3.57e-6 2.08e-5 &
      7.14e-5 1.18e-4 1.43e-4 1.47e-4 1.47e-4 1.54e-4
M1 1001 .0093 $H concrete
    8016 .0463 $O
    14000 .00992 $Si
    20000 .00883 $Ca
    6000 .0065 $C
M2 7014 78.09 $N air
    8016 20.95 $O
    18000 .93 $Ar
M3 1001 16.87 $H soil
    8016 27 $O
    13027 1.976 $Al
    14000 8.963 $Si
CTME 240

```

In the data cards, the source, the tally, the fluence-to-dose equivalent conversion function, the materials, the dxtran variance reduction and the time cutoff are defined. This is all of the input file. Simple as it looks but each parameter specified is subtle.

It has been assumed that the floor is 20 cm thick and has the same composition as concrete. The concrete walls and the ceiling are 1 m thick, so are the extra slabs for primary shielding. The treatment room has an area of 8 m x 8 m and the ceiling is 3 m above ground. The passage of the maze is 2 m wide. An isotropic fission neutron source is placed at the centre of the treatment room, 1.5 m above ground. Figure 3-5 shows a 3-D plan of the model. The ceiling is uncovered except for the back wall so that the treatment room is visible. In the next chapter 2-D plans showing the tally points will be given along with simulation data where necessary. For simplicity the 2-D plans will omit the extra concrete slabs required for the shielding of the primary photon beam. The composition of the materials used in this work is given in Table 3-3.

downloaded
ychin.org

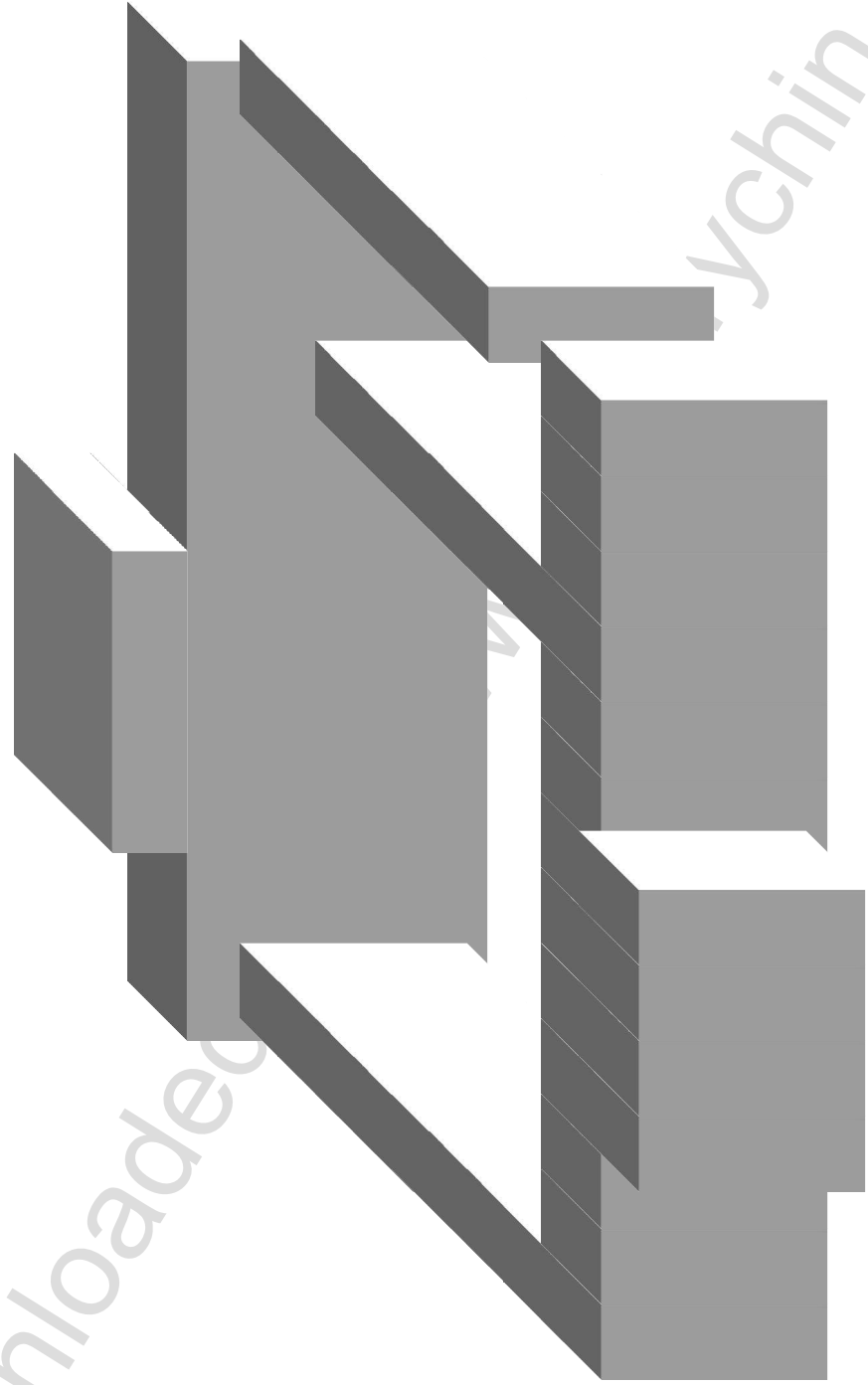


Figure 3-5. A 3-D plan of the simulated model. The ceiling is lifted to show the treatment room.

Table 3-3. Composition of materials.

MATERIAL	ELEMENT	RELATIVE AMOUNT
Ordinary concrete Density=2.43 g/cm ³ Water content=0.14 g/cm ³ [NCR 71, modified]	H	0.115
	O	0.573
	Si	0.123
	Ca	0.109
	C	0.080
Air	N	0.781
	O	0.210
	Ar	0.009
Soil Density=1.25 g/cm ³ [NCR 76, modified]	H	0.308
	O	0.493
	Al	0.036
	Si	0.164

The terms 'fluence', 'fluence rate', 'flux' and 'flux density' deserve attention. In the literature they are used loosely and interchangeably. In this work, the convention used is to let 'flux' be the number of particles per unit area, and 'fluence' be the time derivative of flux. Raw data from MCNP tallies are in 'flux'. After multiplying with the neutron production rate, the answer becomes the fluence, i.e. the number of particles per unit area per unit time.

All simulations assume a neutron production rate of 2×10^9 neutrons per second. The 'points' tallied are all spheres of 10 cm radius. Point detection is difficult to simulate. When the sensitive volume is too small, one can imagine how tiny the probability of any particles crossing there - and thus how long the simulation time required to achieve satisfactory statistics.

Randomness characterises particle transport. As a consequence of the inherent stochastic processes all tallies will be accompanied by fluctuations. All data from simulation will be given along with the corresponding error. All tallies and the corresponding errors will be tabulated as that obtained directly from the output: 5 decimal points for all tallies and 4 decimal points for all errors. For consistency, calculations using empirical formulae will also maintain this number of decimal points. In fact, for most tallies one or two decimal points would be adequate, based on the first significant number of the error. As for dose equivalent tallies, results will be presented in mrem/hr as appears in the original output.

In all simulations, the cross section tables given in Table 3-4 will be used. All are continuous-energy neutron data libraries.

Table 3-3. Neutron data libraries used in simulations.

NUCLIDE IDENTIFICATION NO.	ELEMENT	LIBRARY	SOURCE	DATE OF EVALUATION	TEMPERATURE AT WHICH THE DATA WERE PROCESSED (K)	NO. OF ENERGY POINTS
1001.60c	Hydrogen	endf60	B-VI.1	1989	294	357
6000.60c	Carbon	endf60	B-VI.1	1989	294	978
7014.60c	Nitrogen	endf60	T-2	1992	294	1379
8016.60c	Oxygen	endf60	B-VI.0	1990	294	1609
13027.60c	Aluminium	endf60	B-VI.0	1973	294	2241
14000.60c	Silicon	endf60	B-VI.0	1976	294	2824
20000.60c	Calcium	endf60	B-VI.0	1980	294	2704
18000.35c	Argon	rmccsa	LLNL	before 1985	0	259

The number of energies is the number of energy points on the grid used for the neutron cross sections for that data file. Generally, a higher number of points, thus a finer energy grid, indicates a more accurate representation of the cross sections. ENDF/B-V.# are the Evaluated Nuclear Data Files, a US effort coordinated by the National Nuclear Data Centre at Brookhaven National Laboratory. The evaluations are periodically updated. T-2 indicates evaluations from the Nuclear Theory and Applications group T-2 at Los Alamos National Laboratory. LLNL denotes evaluated nuclear data libraries compiled by the Nuclear Data Group at Lawrence Livermore National Laboratory. The date of evaluation is the year that the evaluation was completed or accepted. The original evaluation date is maintained if corrections made were minor.

Further discussion about neutron cross sections will be given in Chapter 5.

Chapter 4. QUANTIFYING THE HAZARD II: DATA & ANALYSIS

Neutron Dose

The dose equivalents for spheres in air with 10 cm radius centred at a point in the treatment room and at 9 points along the passage of the maze were tallied, as presented in Table 4-1 and Figure 4-1. All are 1.5 metres above ground. The distance for each point is that from reference point T. All tallies assume a neutron production rate of 2×10^9 per second.

Table 4-1. Neutron dose equivalents along the passage of the maze.

POINT	DISTANCE (cm)	NCRP-38		ICRP-21	
		DOSE EQUIVALENT (mrem/hour)	ERROR (fraction)	DOSE EQUIVALENT (mrem/hour)	ERROR (fraction)
T	0	6.81130E+02	0.0032	6.59844E+02	0.0032
A	447	8.51090E+01	0.0120	8.17670E+01	0.0118
B	547	3.44434E+01	0.0172	3.24774E+01	0.0170
C	647	1.56157E+01	0.0232	1.48530E+01	0.0233
D	747	8.43484E+00	0.0336	8.05374E+00	0.0327
E	847	5.10100E+00	0.0381	4.90236E+00	0.0367
F	947	3.30160E+00	0.0237	3.16848E+00	0.0227
G	1047	2.46772E+00	0.0234	2.37862E+00	0.0226
H	1147	2.03998E+00	0.0293	1.95432E+00	0.0276
I	1247	4.59384E-01	0.0377	4.55050E-01	0.0352

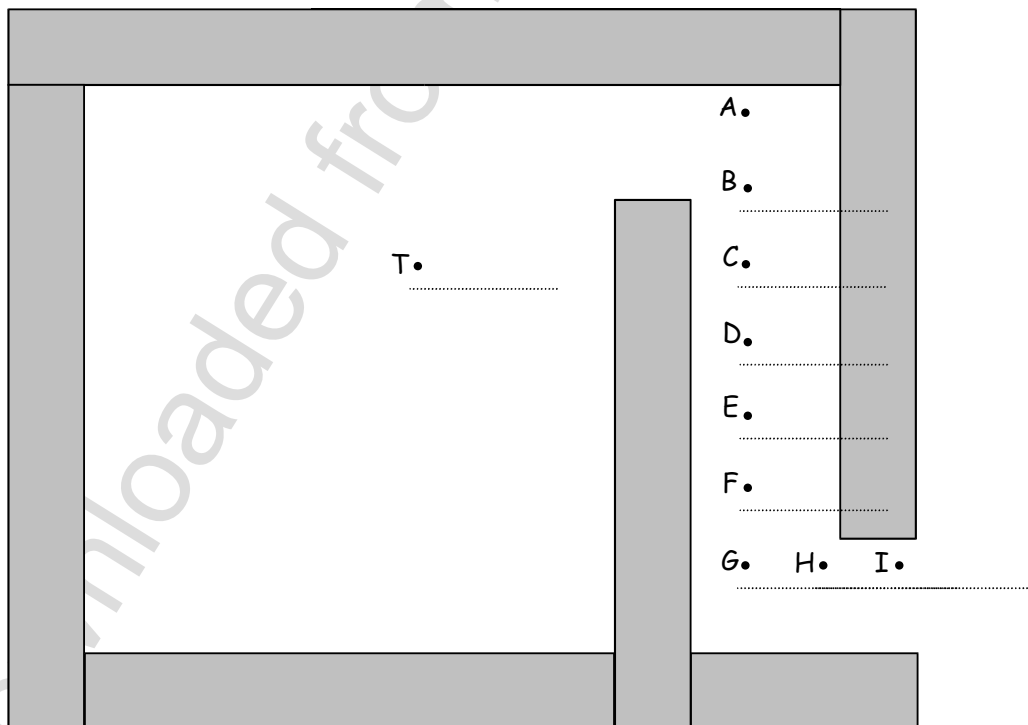


Figure 4-1. Points around which neutron dose equivalents are tallied.

The drop-off for dose equivalents using the NCRP-38 fluence-to-dose equivalent conversion function is shown in Figure 4-2. The dose equivalent just before each bend is found to be a little higher than the best-fit exponential curve. Also, just after each bend, the dose equivalent is below the curve. This shows that bends are good for neutron attenuation. Similar results have been observed in measurements conducted by Lalonde [LAL 97]. A direct comparison between the results of this work and that of Lalonde is given in Figure 4-3.

With a best fit exponential curve shown in Figure 4-2, the average tenth value length (TVL), the distance along the maze passage required for the neutron dose equivalent to drop to its tenth, is calculated to be 403.962 cm. Since the entire passage of the maze is 850 cm in length, the design can be said to achieve over 2 TVLs of dose equivalent attenuation. The dose equivalent dropped by almost a factor of 200 from point A to point I.

Tallies were also made for dose equivalents using the ICRP-21 fluence-to-dose equivalent conversion function. The deviation between the data sets using the NCRP-38 and the ICRP-21 conversion functions is best shown numerically. The ratio of dose equivalents at each point using NCRP-38 conversion functions to those using ICRP-21 conversion functions are tabulated in Table 4-2. The ratios are found to be between 1.01 and 1.06, which means NCRP-38 conversion factors are more conservative, i.e. they always yield a higher dose equivalent.

Table 4-2. Comparison of dose equivalents obtained using NCRP-38 and ICRP-21 conversion functions.

POINT	DOSE EQUIVALENT RATIO $\frac{NCRP-38}{ICRP-21}$
T	1.03
A	1.04
B	1.06
C	1.05
D	1.05
E	1.04
F	1.04
G	1.04
H	1.04
I	1.01

Figure 4-2. Neutron dose equivalents along the passage of the maze.

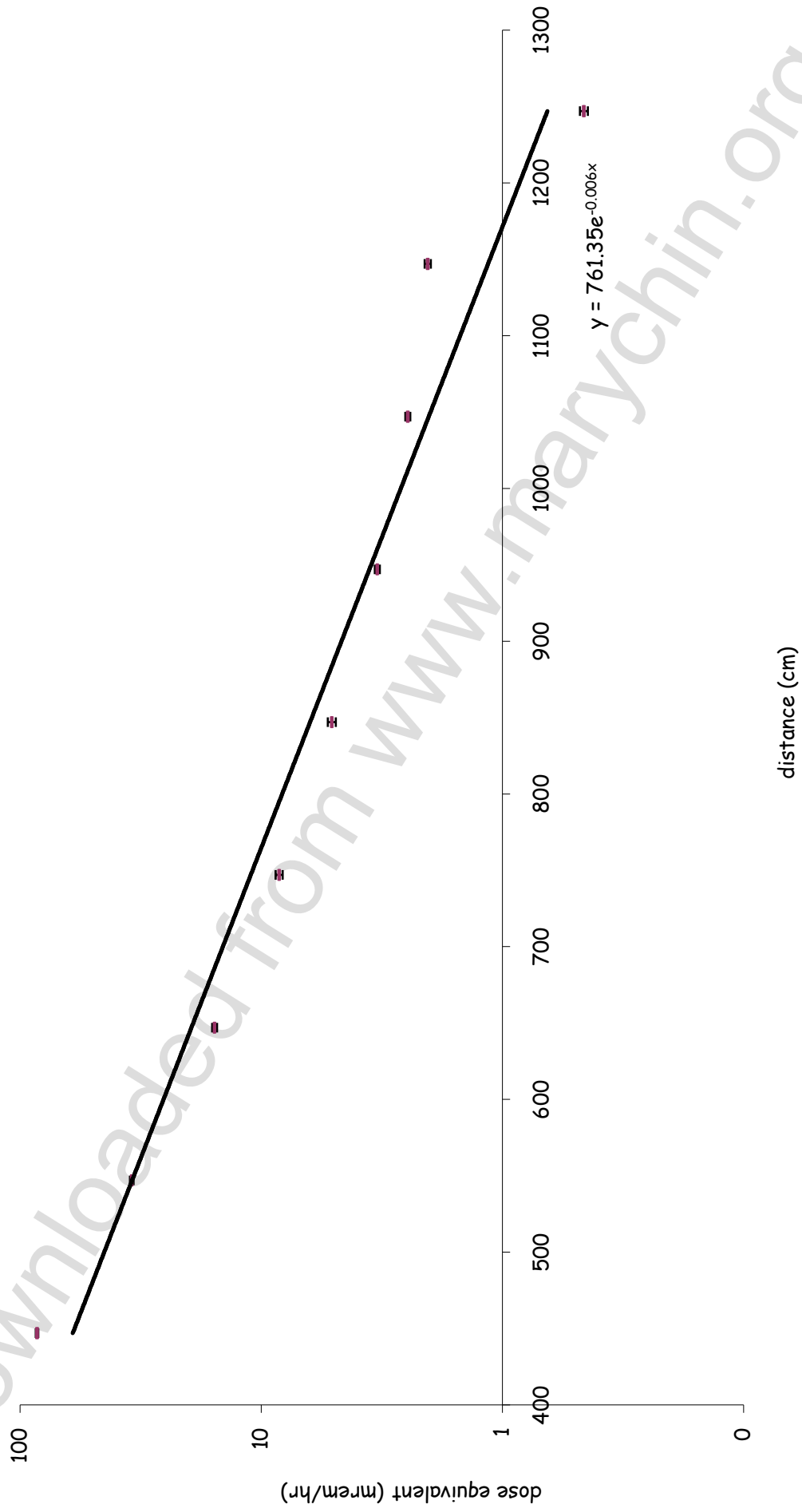
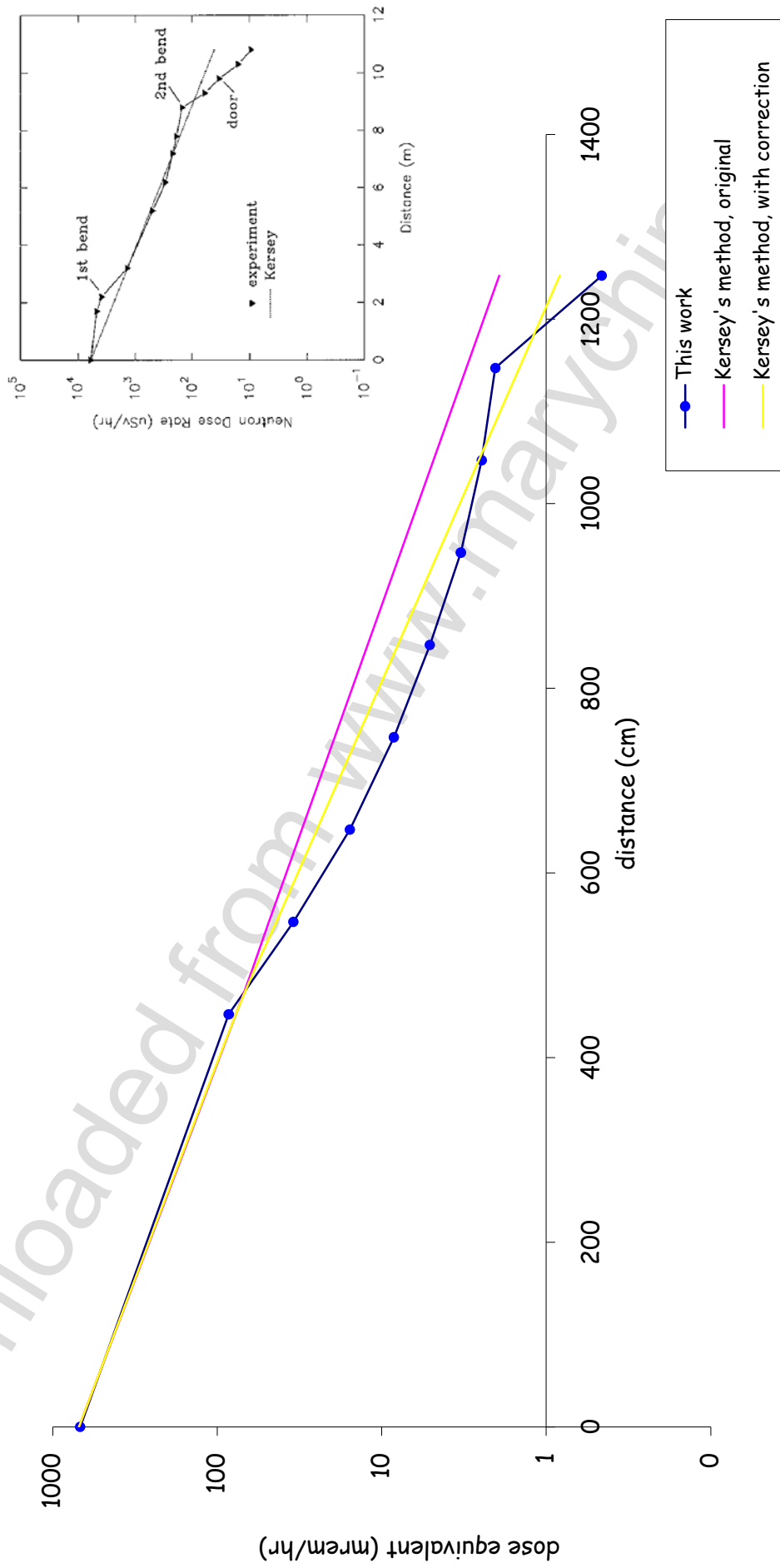


Figure 4-3. Dose equivalents fall-off: a direct comparison with published work [LAL 97].



The dose equivalent fall-off obtained from simulation is then compared with one predicted by calculation. The Kersey method gives an empirical relation that predicts the total neutron dose equivalent at the entrance of the maze. The isocenter of the linac is taken as the neutron source position.

$$H = \left(\frac{d_o}{d_1} \right)^2 10^{-d_2/5} H_o \dots\dots\dots(6)$$

- H = neutron dose equivalent at entrance
- H_o = neutron dose equivalent at a distance d_o from isocentre for neutron output rate of one per second
- d₁ = distance from A to isocentre
- d₂ = distance from A to B in meters

[KER 79, modified]

Based on the geometry of the maze considered in this work, the following can be calculated:

- d₁ = 6.70820 m
- d₂ = 8.00000 m
- d_o = 2.23606 m, the point where H_o is being taken

Taking H_o = 6.81130E+02 mrem/hr (from Table 4-3, NCRP-38 data set), the calculated dose equivalent at the entrance of the maze is then 1.90101 mrem/hr, more than four times the simulated tally of 4.59384E-01 mrem/hr (from Table 4-3).

The calculation was then repeated with a simple modification to equation, by replacing attenuating factor of 5 in equation with 4.03962, which is the TVL in metres found earlier. The formula then predicts a dose equivalent of 7.917729E-01 mrem/hr at the maze entrance, which is still significantly higher than the simulated tally.

It may therefore be concluded that even with modification, the Kersey method over-estimates the dose equivalent at the maze entrance. This over-estimation is no surprise. A study [McG 91] made by McGinley to evaluate the accuracy of the Kersey method gives a ratio of calculated to measured values of up to 2.34. The study was done on 13 different accelerators. The measured and calculated dose

equivalents were compared, yielding the results tabulated in Table 4-3. The last three accelerators in the table were in double-bended maze designs for which the over-estimations are even higher.

Table 4-3. Results from McGinley's study to evaluate the Kersey method.

ACCELERATOR	DOSE EQUIVALENTS AT MAZE ENTRANCE ($\times 10^{-6}$ mSv n/cGy X)		RATIO (CALCULATED/ MEASURED)
	MEASURED	CALCULATED	
1	157	142	0.90
2	23.7	29.2	1.23
3	55.0	55.4	1.01
4	37.1	86.2	2.32
5	13.5	14.0	1.04
6	135	217	1.61
7	42.9	35.1	0.82
8	4.0	3.9	1.0
9	3.3	5.8	1.8
10	15.8	36.9	2.34
11	1.12	2.80	2.5
12	1.96	10.6	5.4
13	0.67	2.62	3.9

[McG 91, modified]

A further simulation was run with a slightly modified geometry. This procedure takes advantage of the flexibility of computer simulations. The wall that formed the second bend near the entrance was knocked off, leaving the maze with a single bend. The neutron dose equivalent at the entrance of the maze, as expected, increased. This proves that a double-bended maze design is more efficient in attenuating neutrons. The dose equivalent for the single bend configuration is found to be nearly twice as high than that for the double bend configuration. Results are shown in Table 4-4, Figure 4-4 and Figure 4-5.

Table 4-4. Neutron dose equivalents at the entrance of the maze for maze configurations with a single bend and a double bend.

MAZE DESIGN	NCRP-38		ICRP-21	
	DOSE EQUIVALENT (mrem/hour)	ERROR (fraction)	DOSE EQUIVALENT (mrem/hour)	ERROR (fraction)
1 bend	9.22062E-01	0.0959	8.91904E-01	0.0945
2 bends	4.59384E-01	0.0377	4.55050E-01	0.0352

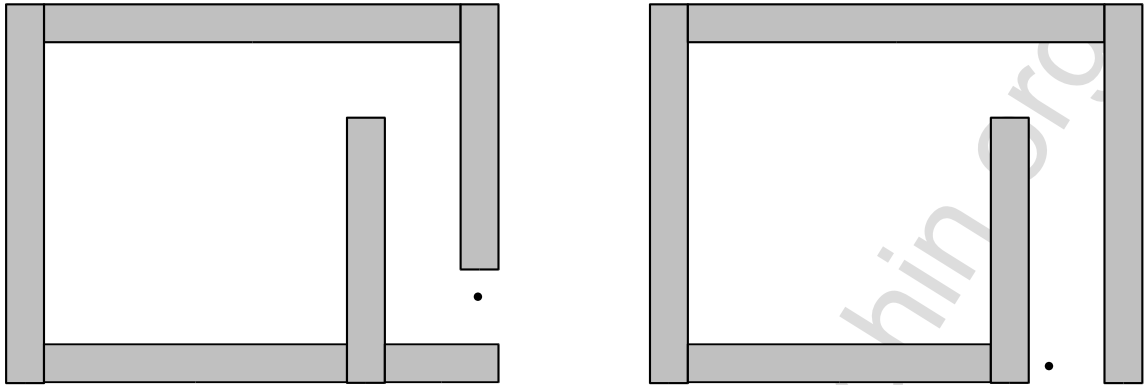


Figure 4-4. Two maze configurations: one with a double bend, one with a single bend. The points tallied for dose equivalents are shown as dots.

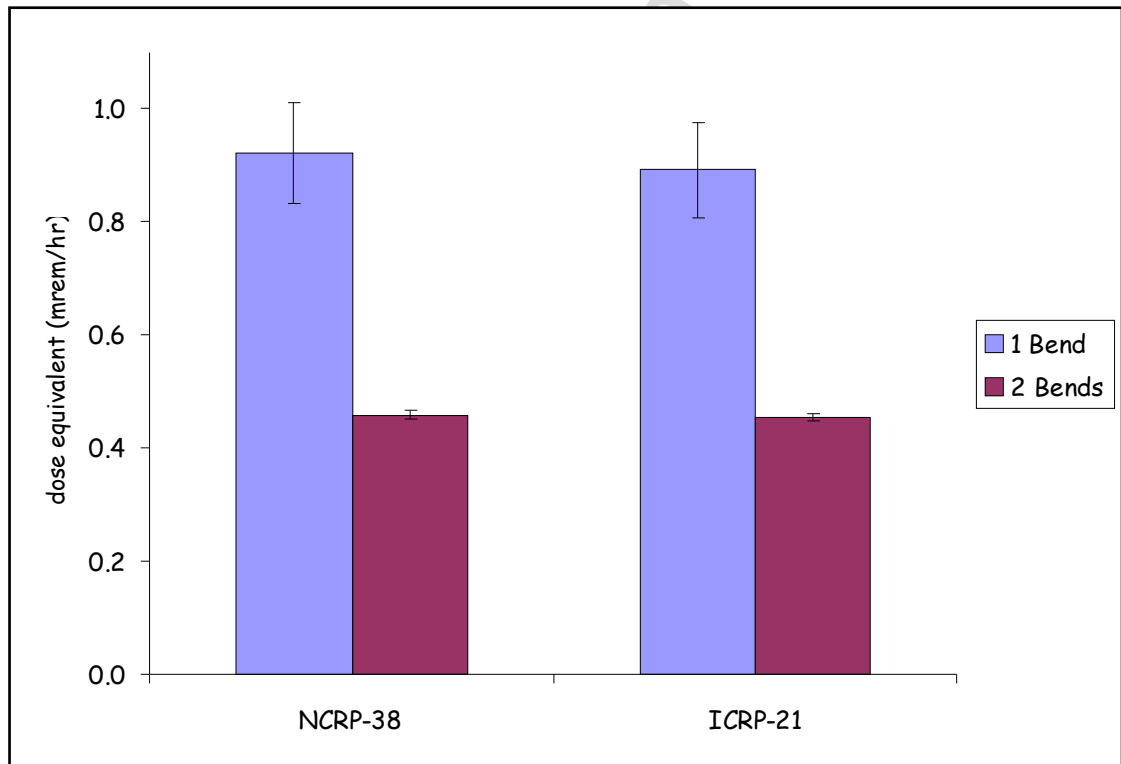


Figure 4-5. Neutron dose equivalents at the entrance of the maze for maze configurations with a single bend and a double bend.

Further modifications were then made. The original height of the ceiling of 3.0 m was varied. Results are tabulated in Table 4-5 and plotted in Figure 4-6.

Table 4-5. Neutron dose equivalents at the entrance of the maze for varying ceiling heights.

MAZE HEIGHT (m)	NCRP-38	
	DOSE EQUIVALENT (mrem/hour)	ERROR (fraction)
2.75	4.56476E-01	0.0313
3.00	4.59384E-01	0.0959
3.25	4.83958E-01	0.0400
3.50	5.85274E-01	0.0541
4.50	6.08950E-01	0.0411

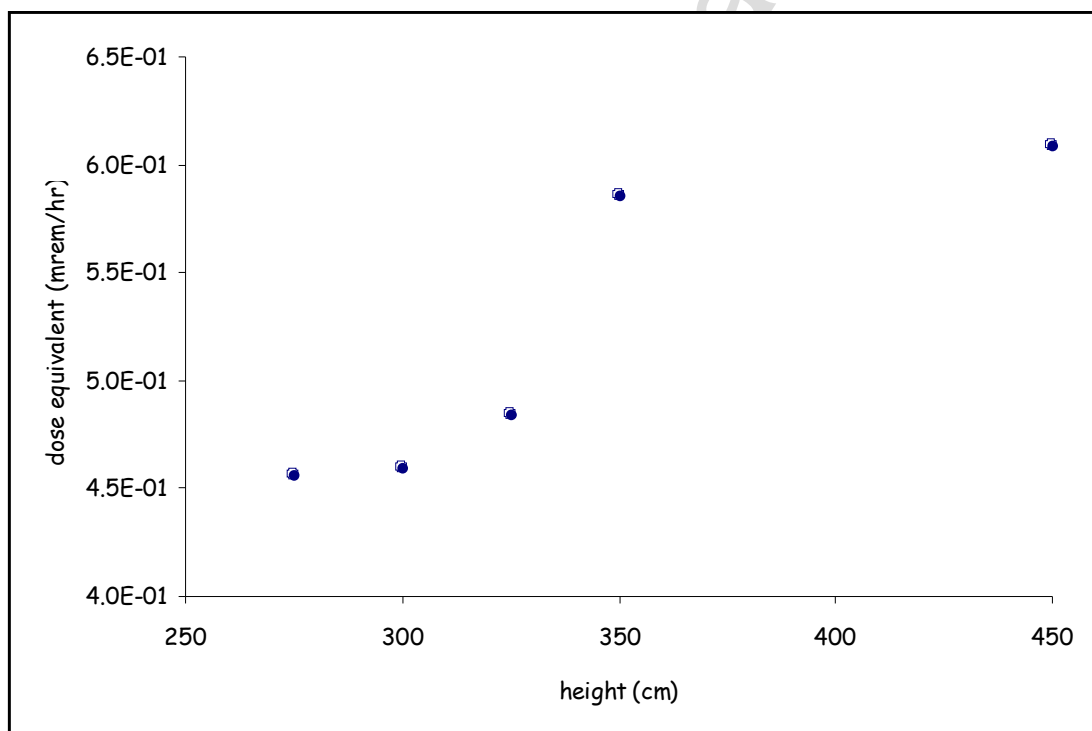


Figure 4-6. Variation of neutron dose equivalent with maze height.

The higher the ceiling, the larger the opening of the entrance hence the higher the dose equivalent. When the height was 25 cm higher, the increase in entrance dose equivalent was less than 1%. When it was 1½ meter higher, the increase was as high as 33%. Due to time limitation, however, the number of data points is insufficient to derive any mathematical relation. This should be a very interesting work to be continued with. The relation may be polynomial. The same could be expected for varying entrance width if the cross-sectional area of the entrance is the determining factor. On the other hand, the effect of neutron backscattering is

expected to increase when the ceiling is low. It should be very interesting to see how these two opposing effects contribute to the resultant dose equivalent.

Neutron Fluence

The neutron fluence in a treatment room does not obey the inverse square law. This is due to the scattering effects from the walls. That is, the bouncing-around of neutrons, without losing much energy, within the barriers. Additionally, the total number of neutrons is not conserved because there are losses due to capture and also build-ups due to (n,2n) interactions.

To illustrate the deviation from the inverse square relation, two simulations were run to tally the fluence at increasing distances from a fission source: one with concrete walls in place and the other without. Table 4-6 shows the data, Figure 4-7 illustrates the geometry. As shown in Figure 4-8, the fluence with concrete walls deviates far from the inverse square relation while that without concrete walls remains close to the inverse square curve.

Instead, the neutron fluence in a treatment room can be expressed in the following:

$$\phi_{dir} + \phi_{scat} + \phi_{th} = \frac{aQ}{4\pi R^2} + \frac{5.4aQ}{S} + \frac{1.26aQ}{S} = aQ \left(\frac{1}{4\pi R^2} + \frac{6.66}{S} \right) \dots\dots(7)$$

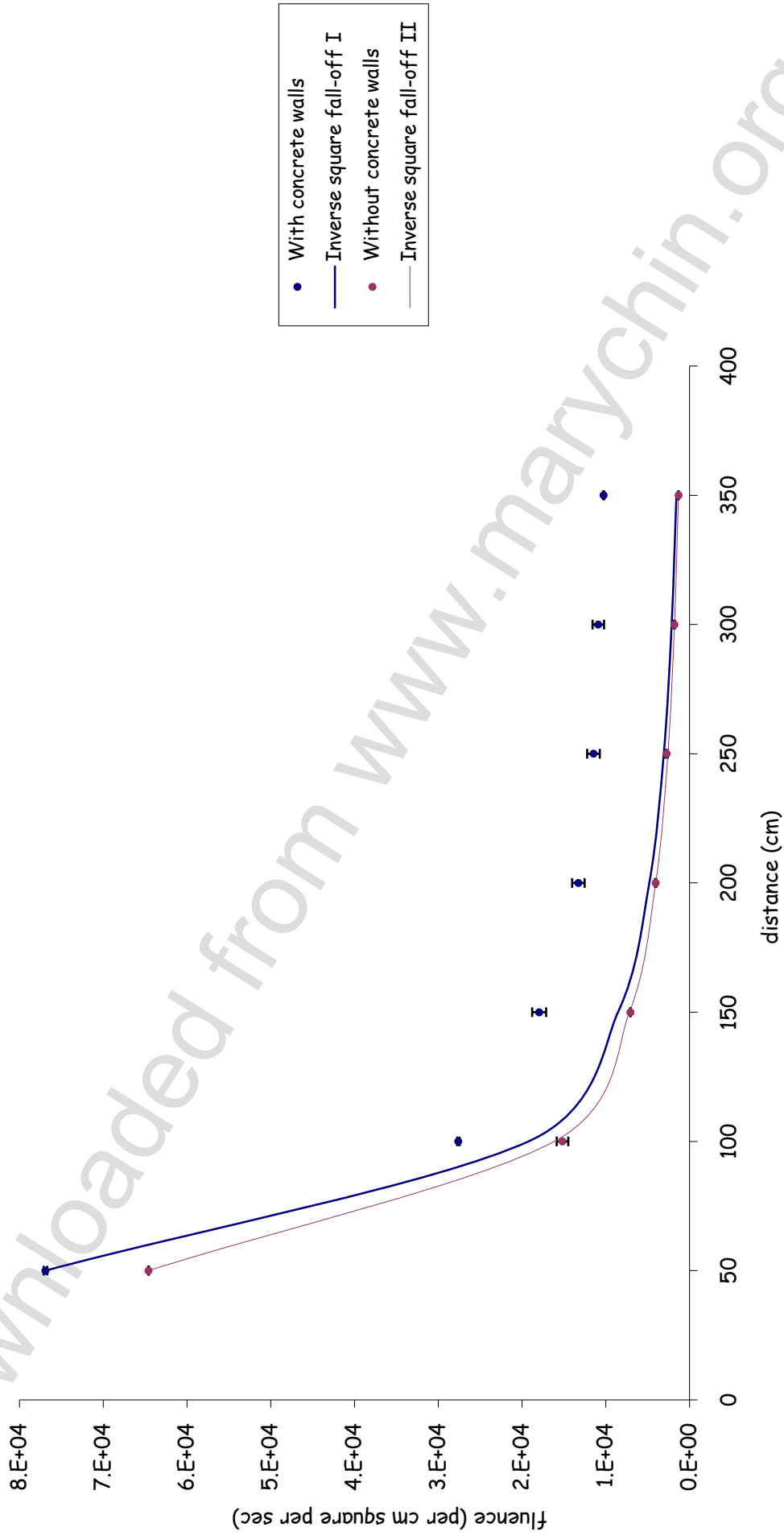
[McC 79, modified]

- a = transmission factor of head shielding:
1.0 for lead and 0.85 for tungsten [NCR 84]
- Q = neutron source strength in number of neutrons per Gy⁻¹ x-ray at isocentre
- R = distance from source in cm
- S = surface area of treatment room in cm²,
which is 1280096 cm for the geometry considered here

The total fluence being made up of three components: the direct fluence, the scattered fluence and the thermal fluence. The relation could be used to predict the fluence by substituting values into Q and a, leading to values that could then be contrasted against the tallied values of fluence from simulation. This, however, would require guess values of Q and a which might not be appropriate for the bare fission source simulated here. Hence, such an attempt will not be made.

Table 4-6. Neutron fluence with and without concrete walls.

Figure 4-8. Variation of fluence with distance.



DISTANCE (cm)	With concrete walls		Without concrete walls	
	FLUENCE (cm ⁻² sec ⁻¹)	ERROR (fraction)	FLUENCE (cm ⁻² sec ⁻¹)	ERROR (fraction)
50	7.69014E+04	0.0028	6.45918E+04	0.0006
100	2.76028E+04	0.0051	1.51693E+04	0.0455
150	1.79579E+04	0.0464	7.06572E+03	0.0005
200	1.32725E+04	0.0560	4.04918E+03	0.0197
250	1.14709E+04	0.0658	2.73088E+03	0.0501
300	1.08954E+04	0.0631	1.81400E+03	0.0354
350	1.02509E+04	0.0059	1.31761E+03	0.0016

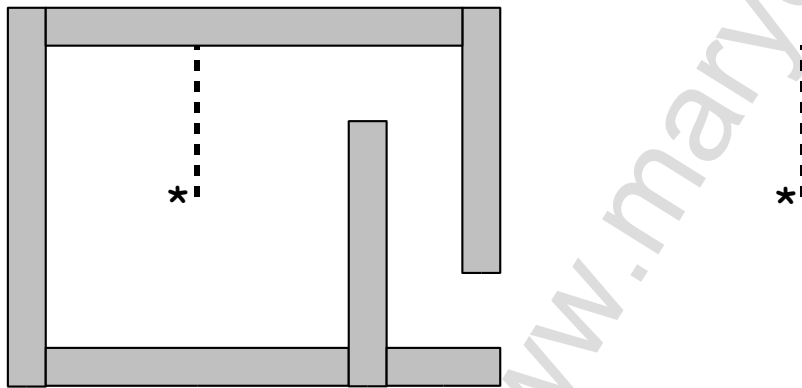


Figure 4-7. Two fission sources: one surrounded by concrete walls, one not. The line along which neutron fluences are tallied is shown as dotted lines.

Instead of imposing values of wild guesses unto Q and a , an alternative approach is taken here - that is, to use the tallied values of fluence obtained from simulation to obtain the value of Q by calculation. Using the relation, an averaged Q can be calculated based on the data from Table 4-6. The averaged Q is 2.25×10^{12} n Gy⁻¹ x-ray if the head shield were made of tungsten, and 1.91×10^{12} n Gy⁻¹ x-ray if it were made of lead.

In fact, this calculation of the neutron source strength by working backwards using the tallied fluences from simulation, tells exactly what a bare fission source actually represents. It either represents a tungsten head shield with a neutron source strength of 2.25×10^{12} n Gy⁻¹ x-ray, or a lead head shield with a neutron source strength of 1.91×10^{12} n Gy⁻¹ x-ray. This calculation is shown in Table 4-7. These values may be compared with published values given in Table 4-8. The values actually indicate a close approximation of the bare fission source to the Varian linac model C 1800 operating at 18 MeV.

Table 4-7. Calculated values of neutron source strength.

FLUENCE (cm ⁻² sec ⁻¹)	NEUTRON SOURCE STRENGTH Q (x 10 ¹² n Gy ⁻¹ x-ray at isocentre)	
	Tungsten head	Lead head
7.69014E+04	2.44	2.08
2.76028E+04	2.47	2.10
1.79579E+04	2.42	2.05
1.32725E+04	2.17	1.85
1.14709E+04	2.08	1.77
1.08954E+04	2.11	1.79
1.02509E+04	2.06	1.75
<u>Average</u>	<u>2.25</u>	<u>1.91</u>

Table 4-8. Published values of neutron source strength.

VARIAN LINACS	NEUTRON SOURCE STRENGTH Q (x 10 ¹² n Gy ⁻¹ x-ray at isocentre)	REFERENCE
C 1800, 18 MeV	2.27	McGinley 1988
C 1800, 15 MeV	1.23	McGinley 1988
C 1800, 10 MeV	0.06	McGinley 1988
C 1800, 18 MeV	2.9	McCall 1987
C 20, 15MeV	0.93	McCall 1987
C 18, 10 MeV	0.059	McCall 1987

A special note needs to be made regarding the transmission factor a , which is taken to be either pure lead, in which case its value is 1.0 because it hardly attenuates the neutrons, or pure tungsten, in which case the value is 0.85 to account for the fact that it attenuates the neutrons. These are the two cases considered in many literatures. In actual case, however, the head shield is usually made of an alloy of composition which manufacturers are reluctant to disclose. It is neither pure lead nor pure tungsten, in most cases.

Another point to note is the direction along which the tallies were made. The results may differ if the points were taken along different directions. The isotropicity of the neutrons emerging from the treatment head may suffer some distortion after scatter, due to the asymmetry of the treatment room caused by the inner opening of the maze. Although there are suggestions that the scatter effect is uniform throughout the treatment room, the accuracy is not checked in this work. It should be interesting to study this symmetry or assymetry in further work.

Neutron Energy Distribution

The energy distribution of neutrons is modified first by the treatment head and then the maze. The initial distribution is close to that of a fission source and is anisotropic. After penetrating the treatment head, however, the emerging distribution is not the same again and it becomes very nearly isotropic. Modifying effects of the energy distribution by the accelerator head can be complex as a number of structures, each with different composition, are involved. Adding to this complexity is the asymmetry of the wedge filter, the secondary collimators and the multileaf collimator.

Two represented models [NCR 84] of a treatment head were simulated in this work: a spherical shell of lead with thickness 15 cm, and a spherical shell of tungsten with thickness 10 cm.

Four sets of energy distributions were tallied: (i) energy distribution of a fission source in empty space; (ii) energy distribution of a fission source in air; (iii) energy distribution outside the lead spherical shell and (iv) energy distribution outside the tungsten spherical shell. The data is presented in Table 4-9, Table 4-10 and Figure 4-9.

Table 4-9. Energy distributions of a fission source in void and in air.

ENERGY BIN	IN VOID		IN AIR	
	FLUENCE (cm ⁻² sec ⁻¹)	ERROR (fraction)	FLUENCE (cm ⁻² sec ⁻¹)	ERROR (fraction)
<0.025eV	0.00000E+00	0.0000	0.00000E+00	0.0000
0.025~1eV	0.00000E+00	0.0000	0.00000E+00	0.0000
1eV~1keV	9.94702E+01	0.0803	2.66702E+01	0.0352
1keV~0.1MeV	9.85152E+04	0.0025	2.47320E+04	0.0012
0.1~1MeV	1.99810E+06	0.0005	5.00496E+05	0.0002
1~10MeV	4.26034E+06	0.0002	1.06534E+06	0.0001
10~20MeV	9.13906E+03	0.0084	2.26632E+03	0.0038

Figure 4-9. Modifying effects on the energy distribution by the treatment head.

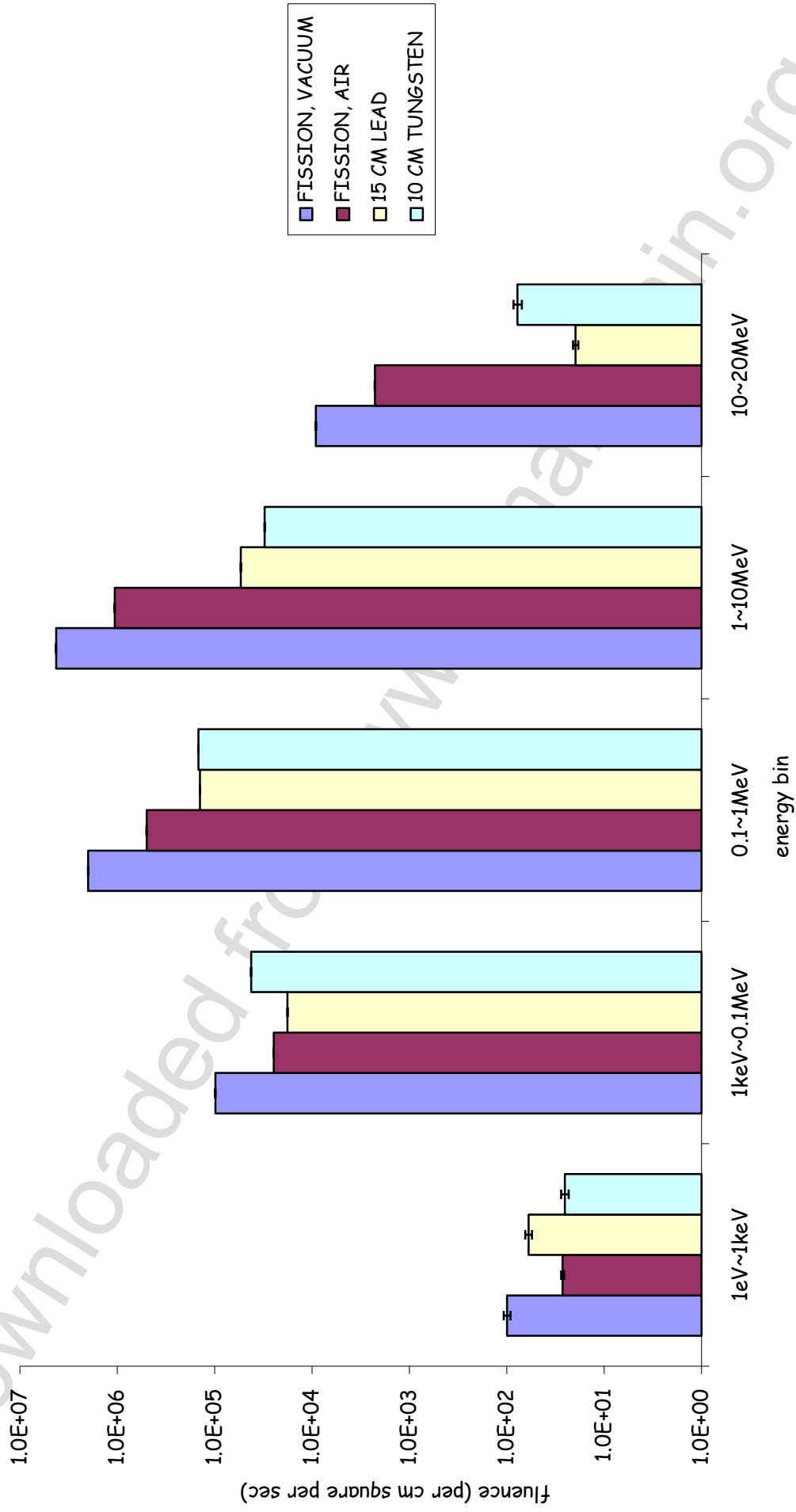


Table 4-10. Energy distributions outside the lead and tungsten models of the treatment head.

ENERGY BIN	LEAD		TUNGSTEN	
	FLUENCE (cm ⁻² sec ⁻¹)	ERROR (fraction)	FLUENCE (cm ⁻² sec ⁻¹)	ERROR (fraction)
<0.025eV	0.00000E+00	0.0000	0.00000E+00	0.0000
0.025~1eV	0.00000E+00	0.0000	0.00000E+00	0.0000
1eV~1keV	5.98012E+01	0.0795	2.53698E+01	0.0893
1keV~0.1MeV	1.78595E+04	0.0041	4.23136E+04	0.0050
0.1~1MeV	1.41291E+05	0.0010	1.46989E+05	0.0024
1~10MeV	5.38846E+04	0.0014	3.06322E+04	0.0038
10~20MeV	1.96276E+01	0.0624	7.75974E+01	0.0987

The presence of air depletes the fluence in every energy bin. It is obvious that the energy distribution after penetrating the treatment head is different for both the models: the fluence in the lowest energy bin increased while for the higher energy bins, the fluence decreased. It may therefore be concluded that using a fission source as the effective neutron source from a medical linac is not accurate.

The two models itself are clearly approximates as well, since both produced slightly different energy distributions while what they are supposed to represent is the same.

To check the changes in the spectrum of neutrons as they travel around the maze, neutron fluence for different energy bins was tallied at different points using MCNP. The results are tabulated in Table 4-11.

As evident from Figure 4-10, the high-energy components of the neutrons deplete dramatically as neutrons travel along the passage of the maze. Since neutron capture is not immediate, there is a gradual removal of fast neutrons, along with a substantial buildup of epithermal and thermal neutrons. The contribution of neutron fluences in each energy bin to the total neutron fluence at the entrance of the maze were then calculated using the data from Table 4-11, and is given in Table 4-12.

Figure 4-10. Modifications of energy distribution by the maze.

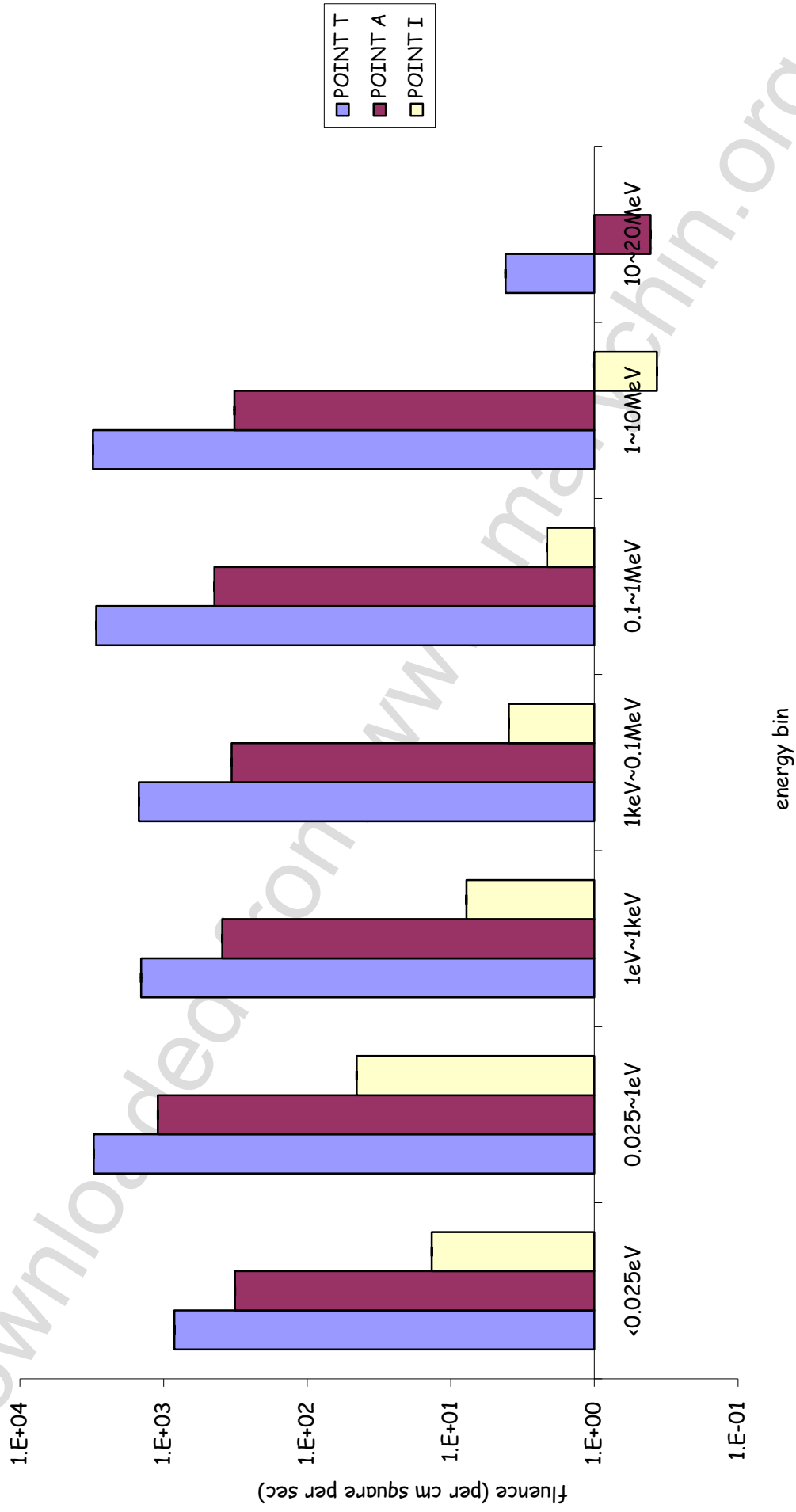


Table 4-11. Fluences in energy bins at three different points.

ENERGY BIN	In Treatment Room		At Inner Bend		At Maze Entrance	
	FLUENCE (cm ⁻² sec ⁻¹)	ERROR (fraction)	FLUENCE (cm ⁻² sec ⁻¹)	ERROR (fraction)	FLUENCE (cm ⁻² sec ⁻¹)	ERROR (fraction)
<0.025eV	8.39808E+0 2	0.0129	3.17838E+02	0.0218	1.35596E+01	0.0369
0.025~1eV	3.06430E+0 3	0.0097	1.09637E+03	0.0167	4.52610E+01	0.0296
1eV~1keV	1.43588E+03	0.0109	3.89730E+0 2	0.0264	7.78118E+00	0.0609
1keV~0.1MeV	1.48614E+03	0.0111	3.34964E+0 2	0.0236	3.93366E+0 0	0.0730
0.1~1MeV	2.93810E+03	0.0060	4.42824E+0 2	0.0187	2.13576E+00	0.0818
1~10MeV	3.09888E+0 3	0.0044	3.20874E+0 2	0.0149	3.66622E-01	0.1526
10~20MeV	4.16120E+00	0.1231	4.05482E-01	0.2352	0	0

Table 4-12. Contribution of each energy bin to the total neutron fluence at the maze entrance.

ENERGY BIN	CONTRIBUTION (%)
<0.025eV	19
0.025~1eV	62
1eV~1keV	11
1keV~0.1MeV	5
0.1~1MeV	3
1~10MeV	1
10~20MeV	0

Secondary Photons

For all simulations done in this work, no photon source is applied. The only radiation source applied is a neutron fission source. Photons are produced, however, when the neutrons undergo (n,γ) interactions and inelastic scattering. This section attempts to show the presence of these secondary photons.

When neutrons impinge on the walls and the air in the room, the materials can be activated. As a result, secondary photons are produced. By simulation, photon fluence was found to be present in the walls and in the air, as listed in Table 4-13 and shown in Figure 4-11 and Figure 4-12.

Table 4-13. Secondary photon fluence in concrete walls and room air.

REGION	FLUENCE ($\text{cm}^{-2} \text{sec}^{-1}$)	ERROR (fraction)
W	5.064560E+02	0.0114
M	6.115000E+02	0.0123
E	8.950660E+01	0.0335
S	6.203220E+02	0.0115
N	5.044480E+02	0.0109
D	1.516830E+01	0.0967
A	2.092600E+03	0.0064

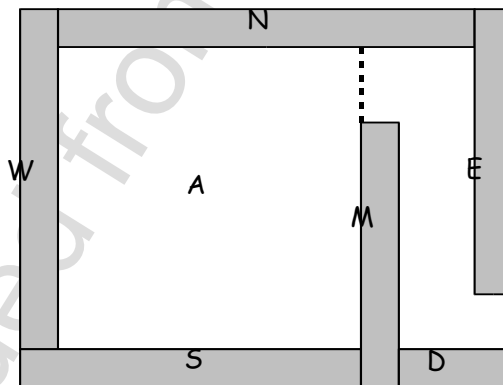
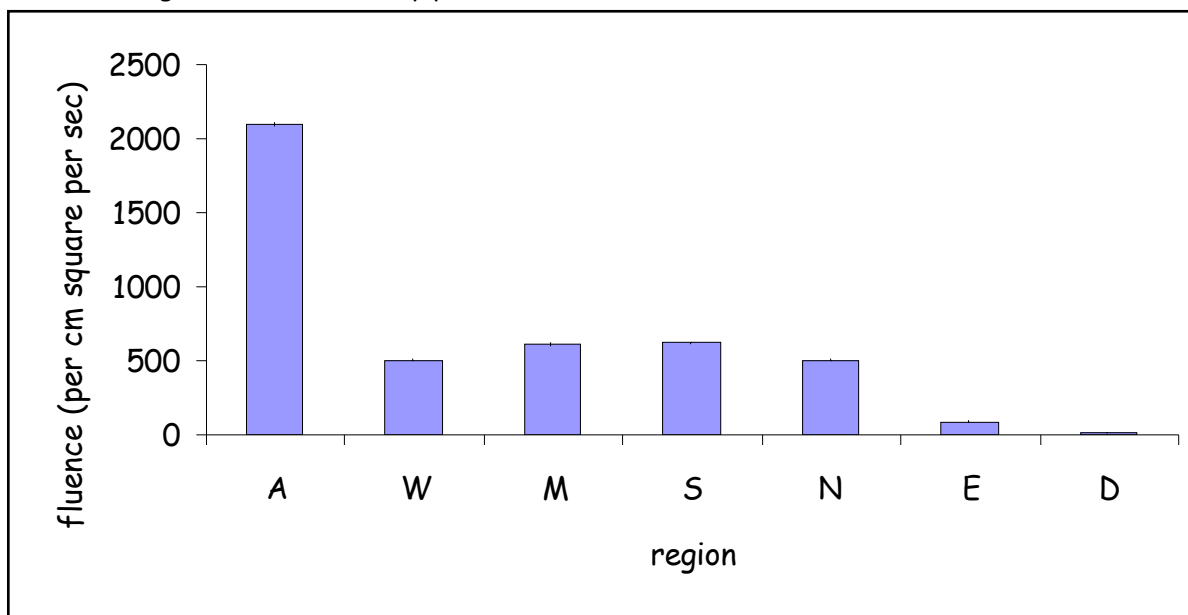


Figure 4-11. Activated regions of concrete walls and room air tallied for photon fluence.

Figure 4-12. Secondary photon fluence in activated walls and in room air.



The secondary photons produced from activation give rise to another source of dose. Secondary photons are not only present inside the treatment room, but also at the entrance of the maze. The dose equivalent at the entrance of the maze due to secondary photons is tallied and is given in Table 4-14. Two sets of conversion factors were used: one of 1977 ANSI/ANS, and the other of ICRP-21. The latter predicts a lower dose equivalent than the former.

Using the neutron dose equivalent found earlier in Table 4-1, dose equivalents due to neutrons and secondary photons, converted using ICRP-21 conversion factors, can be compared. That due to secondary photons is found to be nearly a ninth of that due to neutrons.

Table 4-14. Dose equivalent due to secondary photons at maze entrance.

1977 ANSI/ANS		ICRP-21	
DOSE EQUIVALENT (mrem/hour)	ERROR (fraction)	DOSE EQUIVALENT (mrem/hour)	ERROR (fraction)
5.36184E-02	0.0276	4.83606E-02	0.0285

Chapter 5. QUANTIFYING THE HAZARD III: ERRORS & RELIABILITY

Variance Reduction

Variance reduction is a potential solution when a simulation run over a tolerable length of computing time gives hopeless results. A hopeless situation would be where the precision of the results is very low. For example, the error bar can be as tall as the histogram. Or, worse still, the tallies can all be zero when they should not be. Tallies are the results the user wants from the simulation, e.g. flux over a cell or across a surface. These are the quantities of interest requested by the user, i.e. the information to be obtained from the simulation.

A deep penetration problem is one of such hopeless situations. The simulation of a shield and to tally for particle transmission through the shield, as in the simulation done here, is a good example of a deep penetration problem. This will be elaborated later.

In mathematical terms, variance reduction sets out to decrease the relative standard deviation of the mean, which is proportional to the square root of the history variance and inversely proportional to the square root of the number of particles. So one can try to decrease the history variance, or to increase the number of particles, or even more ideally, both - all within a certain time limit. Increasing the number of particles within a set time limit means decreasing the time per particle history. Unfortunately, a seesaw effect often plays up: once the history variance is held low, the time per particle history inevitably goes up, and vice versa. A clever variance reduction scheme obtains a good bargain by give-and-take: have a low history variance and let the time per particle history go up a little - but just not too much, so that there is an overall win. The another option would be to lower the time per particle history and let the history variance go up a little - just not enough to cancel the gain.

In short, variance reduction reduces the variance. That is, it improves the precision. It, however, only improves the accuracy to a certain extent. The accuracy depends on many other factors, as given in Table 5-1.

Table 5-1. Factors affecting accuracy.
[BOO 85, modified]

Code factors	Physics and models Data uncertainties Cross-section representation Coding errors
Problem-modelling factors	Source model and data Geometrical configuration Material composition
User factors	Input errors Variance reduction abuse Checking the output Understanding the physical measurement

The philosophy of variance reduction is to reduce the amount of computing time required in order to obtain results of acceptable precision. It works by changing the conventional random walk sampling. Instead of sampling all particles non-preferentially, it samples preferred particles, i.e. those that would score. To score is to contribute to the results. A Monte Carlo estimate of the reaction rate is called the score. Every simulated event make a contribution to the score, even when it is zero - which happens most of the time.

For instance, if the desired result is to detect neutron flux at a certain point away from a source, there is no point following particles that go further and further away in the opposite direction and never come anywhere near the tally region. Without variance reduction, time would be wasted following these non-contributing particles. With variance reduction, the random walk sampling forget about these particles altogether.

There are many different variance reduction techniques. Some forget about non-contributing cells. Some take a step further by creating pseudo-particles that score. Some 'push' the particles in a favoured direction and help them enter the region where the detector is waiting for them. In Monte Carlo language, variance reduction techniques bias the sampling, but later compensate the bias before giving the final results. In layman's term, to bias is to cheat and to compensate is to cover up so that there is no trace of cheating in the final results.

The way to compensate is by adjusting the statistical weight of the particles. The 'weight' in Monte Carlo language is the number of physical particles the Monte Carlo particle represents. The physical particles represented by a Monte Carlo particle are transported in the same, one random walk. For most of the techniques, MCNP takes care of the compensation automatically but it may not be perfect. The user has to take care not to overbias.

The variation in the number of tracks scoring, but not the variation in particle weight, determines the history variance. However, it has been empirically shown that large weight fluctuations do affect tallies deleteriously.

To apply variance reduction to a problem, the first step is to diagnose the problem: why is the tally poor? This can usually be identified by diagnosing the output of an initial run - which requires some skill and experience. Perhaps there is a penetration problem where there are highly attenuating materials between the particle source and the tally region, or there is a difficult angular turn in-between.

The second step is to choose the appropriate variance reduction technique(s). The third step is to select the optimum parameter(s) for each particular technique. For example, if the technique chosen is to bias the source direction, then the angle and the reference direction must be specified as the parameters. Different techniques require different parameters. Some techniques do not work well together. There is hardly any standard criterion for choosing both the technique and the parameters. For a particular problem, trial-and-error is always a necessary part of the process.

The first difficulty in the simulation done in this work is the concrete walls of the bunker. A deep penetration problem, as mentioned earlier. The concrete barriers shield the neutrons. Some, but a small fraction, of the total neutrons do penetrate the concrete barriers. In an actual physical situation, a small fraction of neutrons are thus expected over the other side of the concrete walls, i.e. next-door to the treatment room. Simulations over a reasonable length of time, however, would give zero tallies, which imply there were no neutrons detected there. This happens because first, a meter of a 2.43 g/cm^3 concrete is difficult to penetrate, and

second, the particles lose energy while penetrating the concrete. The diagnosis of the problem is: extensive computing power and time is exhausted by following too many particles which spend a long time losing weight (defined later) and losing energy within the concrete wall. Variance reduction is necessary.

Geometry splitting and Russian roulette are used as a combined variance reduction technique. This application makes the code definition of the geometry subtle. The way the technique is applied is first to divide each piece of concrete walls into thin slices of thickness 10 cm across its thickness. Since each wall is 1 m-thick, each piece of wall is now made up of 10 slices. Each slice is then assigned a value of importance, which is to increase progressively from the slice nearest to the source outwards, for example 2, 2, 4, 4, 8, 8, 16, 16, 32 and 32. 10 slices of 10 cm each but not 5 slices of 20 cm - the reason is to avoid big jumps of importances between adjacent slices - which may cause weight fluctuations. The technique operates this way: as a track crosses from one slice to the neighbouring one, it is transported as usual if the importances of the two slices are the same. On the other hand, if it enters a slice with a higher importance it will be split according to the importance ratios. If, however, it enters one with a lower importance, a Russian roulette is played: with probabilities defined by the importance ratio it may either survive or die. The effect is therefore to have particles penetrate the slices, i.e. there is a preferential push of particles towards the outer surface of the concrete wall.

By assigning the importance this way, the slices are made progressively more important the further they are from the source. They are important in the sense that more computing effort would be spent following the histories there. The bias is compensated by adjusting the weights of the tracks.

Energy splitting with Russian roulette is another combined variance reduction technique which is very similar to geometry splitting combined with Russian roulette. The difference that it is done in the energy domain rather than in the geometrical domain. Although this technique increases the number of histories dramatically, it is not used because: 1) It is problem-wide, i.e. in the context of the maze simulated in this work there would just one, universal cutoff energy for the

entire maze - which would not be sensible since for some regions low-energy particles are worth following while for others not; 2) The neutron energy distribution and the neutron dose equivalent are to be tallied here - both are highly sensitive to the population of neutrons in each energy bin.

Energy cutoff is another variance reduction technique avoided here. The reasons are: 1) It is, again, problem-wide; 2) The bias is not compensated; 3) Applying an energy cutoff would mean chopping off a dominant part of the spectrum.

Weight cutoff is used so that no computing effort is spent in vain following extremely low-weight particles which would never contribute to the tally. Unlike energy cutoff which truncates without compensation, weight cutoff is compensated. The weight is increased for particles that survive.

Implicit capture is a technique applied so that all particles survive collisions. It saves the miss when a particle would otherwise be absorbed right before entering the tally region. It is compensated by weight adjustments calculated according to the total cross-section and the absorption cross section.

DXTRAN ('deterministic transport') spheres work wonders in this simulation. They attract source particles and scattered particles into the tally regions. The extra weight created for the DXTRAN particles is compensated by the weight killed as non-DXTRAN particles enter the cell. The drawback is that it slows down the simulation. It is therefore necessary to define dxtran contribution probabilities so that regions that contribute low-weight particles contribute less. To avoid cross-talk and therefore low efficiency, no more than one is used in a single simulation.

The 10 statistical checks

All the results given in this work achieved relative errors below 0.10 (fraction) and have passed all 10 statistical checks. With the condition that all portions of the problem phase space have been sufficiently sampled, the confidence level is reliable.

The parameters computed and produced in the output include:

1. estimated mean
2. relative error
3. variance of the variance
4. history score probability function

Figure 5-1 shows, as an example, part of an MCNP output where the diagnosis of each test is given.

Having passed the 10 statistical checks means:

1. The mean has a random behaviour, which is required since an ideal random quantity should have a normal distribution of values around its average value. In other words, an increasing or decreasing trend over the second half of the run would not be acceptable. Increasing or decreasing trend during the first half of the run is waived in order to allow for the run to become stable.
2. The relative error achieved a fraction lower than 0.10 and it decreased as histories proceeded. For the second half of the run, the relative error had decreased with a rate inversely proportional to the square root of the number of histories.
3. The variance of variance was lower than 0.10 and that over the second half of the run, it decreased monotonically with a rate inversely proportional to the number of histories.
4. The figure of merit (fom) was stable and random. The figure of merit is a measure of efficiency of the computation and is defined as the inverse of the product of the relative standard deviation of the mean and the computing time. Since the first term should be inversely proportional to, and the second should be proportional to the number of histories, the figure of merit is expected to be close to constant for a well-sampled simulation.

Figure 5-1. The 10 statistical checks as appear in a typical MCNP output.

```

=====
results of 10 statistical checks for the estimated answer for the tally fluctuation chart (tfc) bin of tally 64
=====
tfc bin  --mean--  -----relative error-----  ---variance of the variance---  --figure of merit--  -pdf-
behavior  behavior  value  decrease  decrease rate  value  decrease rate  value  behavior  slope
desired  random  <0.10  yes  1/sqrt(nps)  <0.10  yes  1/nps  constant  random  >3.00
observed  random  0.04  yes  yes  0.00  yes  yes  constant  random  10.00
passed?   yes     yes  yes  yes  yes  yes  yes  yes     yes  yes
=====

```

downloaded from www.marychin.org

5. The probability density function reached a slope of at least 3.00, which implies that the level of confidence became more reliable as more histories were run due to increased sampling.

Figure 5-2 demonstrates the process of meeting the demands of these tests as the number of histories proceeds. This example uses the data taken from the output file where the neutron fluence in the treatment room was tallied.

The checks are statistical checks -- they do not check against overbiasing and undersampling. A bad tally may still pass all the 10 checks if the simulation is overbiased or poorly sampled. There are still other sources of uncertainties inherent in the tallies, including the neutron cross sections and the fluence-to-dose conversion factors.

downloaded from www.marychin.org

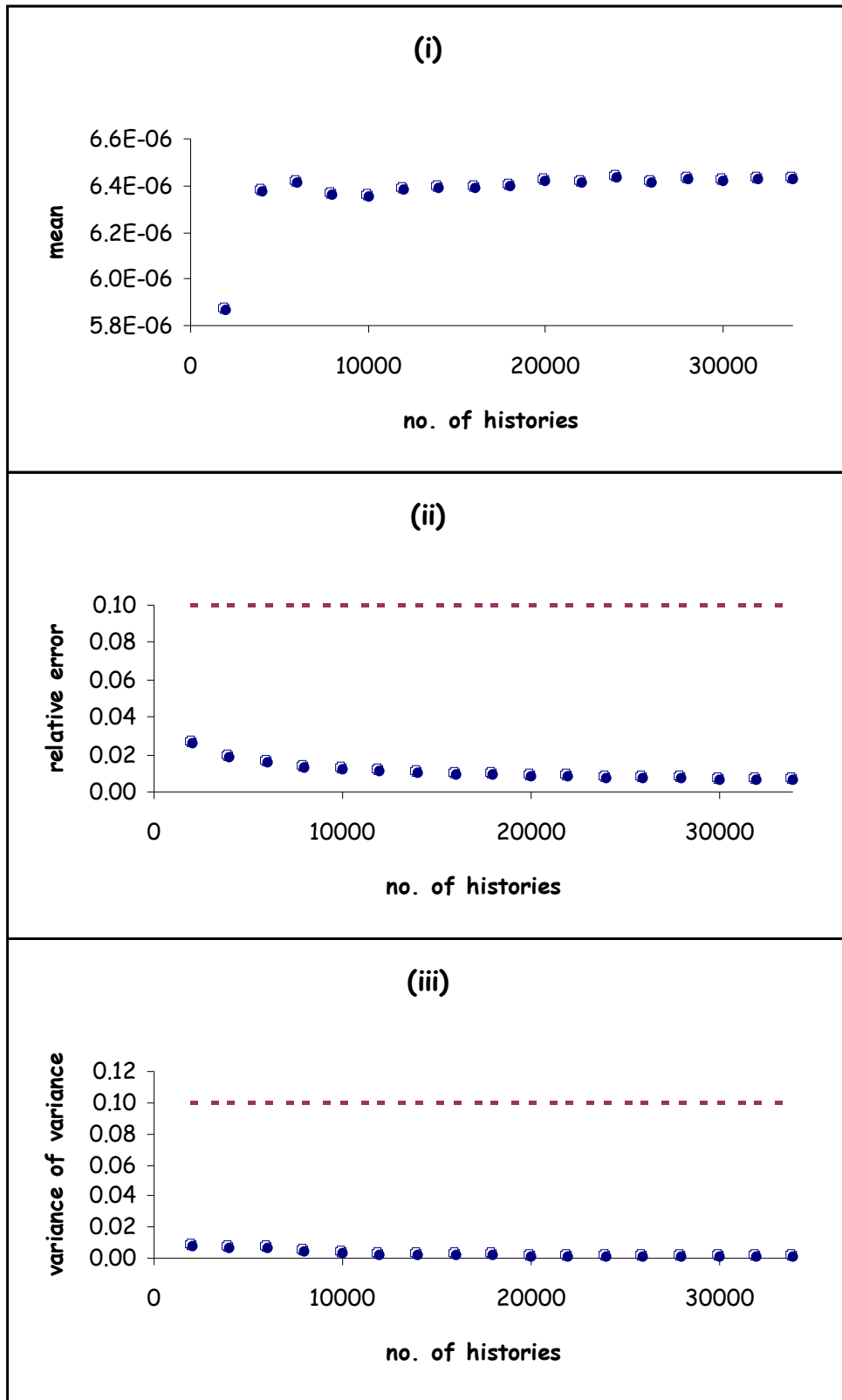


Figure 5-2. The process of passing the 10 statistical checks:
 (i) the mean takes time to settle down;
 (ii) the relative error decreased to an acceptable value below 0.10;
 (iii) the variance of variance achieved a value lower than 0.10.

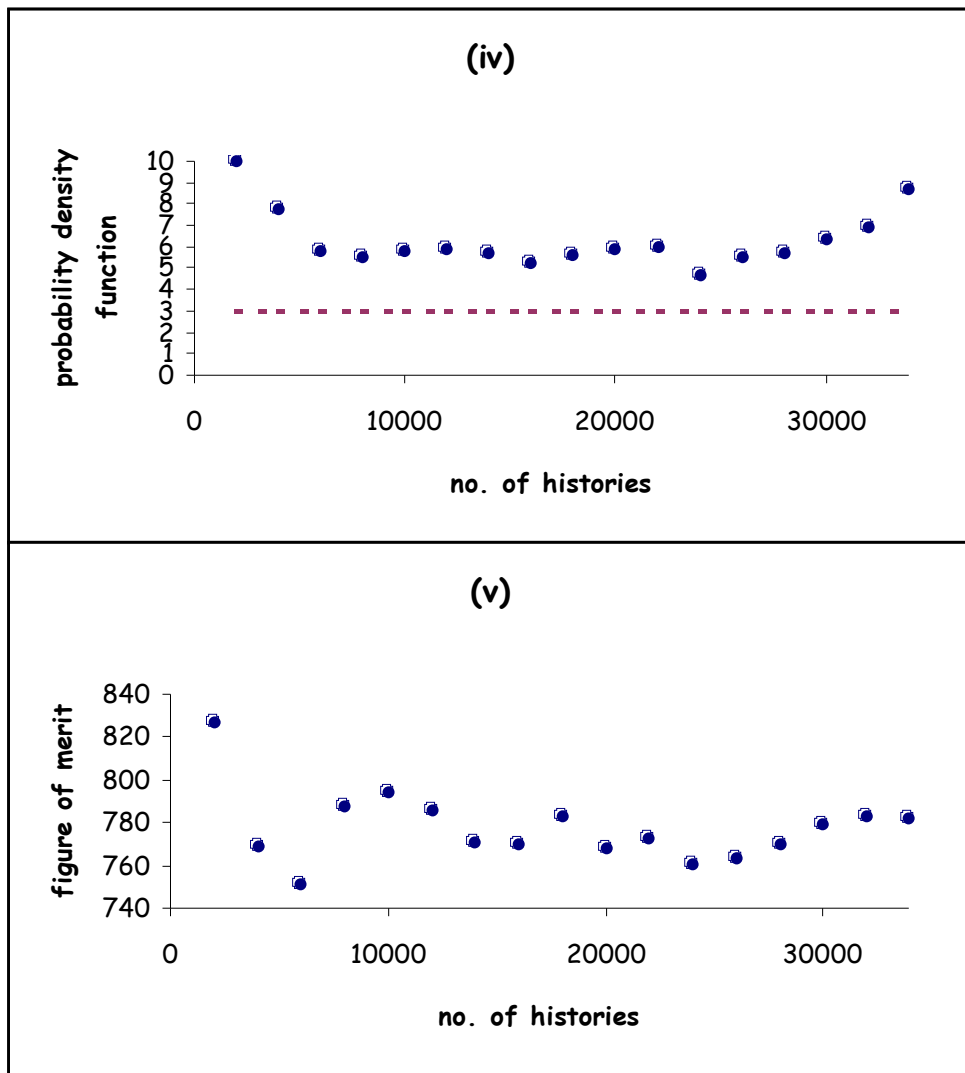


Figure 5-2. (cont'd) The process of passing the 10 statistical checks:
 (iv) the probability density function reaching a slope of over 3.0;
 (iv) the figure of merit becoming stable.

downloaded from

The 2 Dangers

The two dangers of variance reduction are overbiasing and undersampling. Overbiasing does produce deceptive 'well-behaved' tallies, i.e. erroneous tallies that pass all statistical checks. Here is an example. To tally for the dose equivalent at point H, 2 versions of code with different variance reduction scheme were executed. The second had additional applications of energy roulette, source angle bias and source energy bias. Sufficient histories were then run for both versions until they have passed all statistical checks. Both tallies gave values that were not within acceptable range.

The second version is clearly overbiased. This is shown in Figure 5-3. The value of an overbiased tally is way above the value of the tally from the first version. This is the consequence of a bias that is not compensated adequately. That is to say, there are still traces of 'cheating' in the final results. This explains why the overbiased tally is higher, not lower, than the tally from the first version.

As mentioned earlier, undersampling may also yield misleading tallies. The tallies may pass all the statistical checks brilliantly, leaving few clues that anything is amiss. It is the liability of the user not to write a code that undersamples. Undersampling occurs when a region, which would otherwise contribute significantly to the tally, is insufficiently sampled. This happens when the importance or the dxtran contribution probability for that particular region is set too low. This is bad because it neglects regions which are not negligible.

If the sampling frequency or the contribution probability for that region is set to zero, the region is excluded altogether from sampling and no matter how many histories are run, the tally forever appears well-behaved. On the other hand, if the sampling frequency or the contribution probability is non-zero but too low, the tally behaviour would improve with the number of histories - only to a certain stage, after which the performance of the tally would drop. This is when, eventually, some of the poorly sampled region do contribute -- but far from enough to give good statistics. This is also when the user can see some signs of undersampling.

This also implies that for a code that samples poorly, a simulation which has passed all statistical checks after a 10-hour run may fail a 15-hour run. On the contrary, a well-behaved tally that is well sampled would stabilise and improve as more histories were run.

In order to avoid any hidden undersampling in this work, cell importances and dxtran contribution probabilities were never set to zero. The dxtran contribution probability is also set with reference of the number of histories to be run. The user should be prepared to run sufficient number of histories in order to allow at least some particles from the region of lowest probability to contribute. In this case, if the sampling is poor, it will show up in the statistics. Diagnosis, modification and corrections can then be made.

An example of the subtlety of poor sampling will be illustrated here. In the following example, the dose at the entrance of the maze was to be tallied using a dxtran sphere for variance reduction. The contributions from the air in the room and along the passage of the maze were inappropriately set too low. The tally passed all statistical checks when 121650 histories were run. After the 192000th history, however, the tally behaviour started to deteriorate: the slope began to decrease and the FOM began to drop, as shown in Figure 5-4. A decreasing trend in the FOM indicates that a seldom-sampled particle path is significantly affecting the tally result. If simulation were terminated sometime before this began, the output would give a dose equivalent which deviates from the true value but passes all 10 statistical checks.

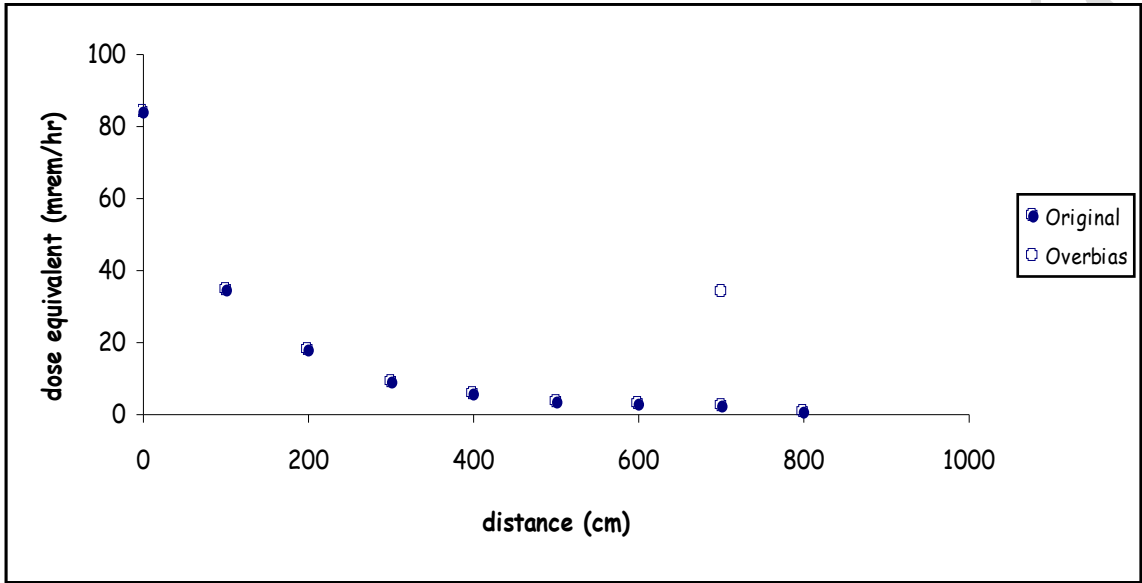


Figure 5-3. An example of overbiasing. The dose equivalent obtained is far from that obtained when there is no overbiasing.

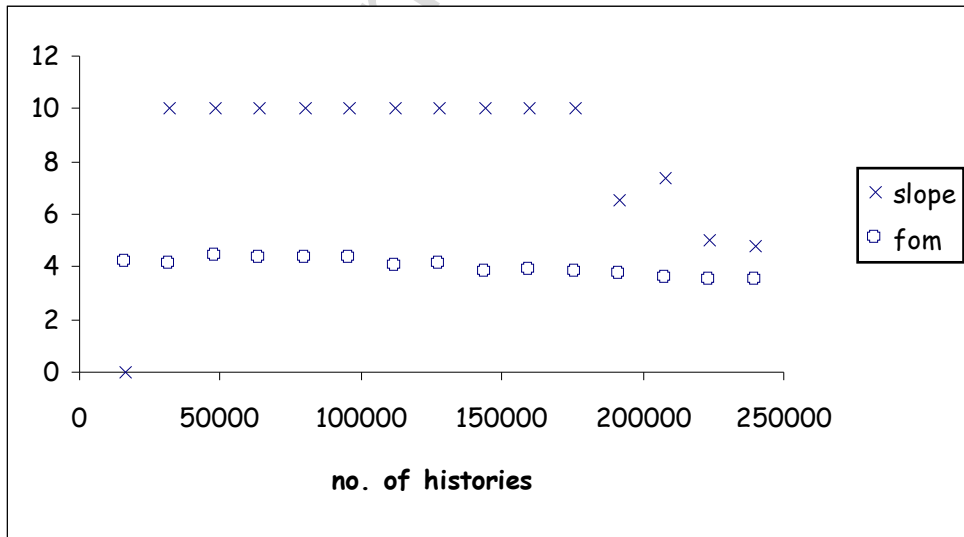


Figure 5-4. An example of poor sampling: the slope and the fom starts to deteriorate when the number of histories approaches 200000.

Reproducibility

The simulation run to tally for the dose equivalent at point B was repeated for 3 times over the same time limit of 60 minutes. The results are given in Table 5-2.

Table 5-2. Results of repeated runs.

RUN	NO. OF PARTICLES STARTED	TALLY RESULT	ERROR	VARIANCE OF VARIANCE	SLOPE	FOM
#1	83519	1.7221E-11	0.0172	0.0031	4.4	56
#2	83496	1.7222E-11	0.0172	0.0031	4.4	56
#3	83496	1.7222E-11	0.0172	0.0031	4.4	56

The repetitions are expected to be well-behaved in the sense that they should not deviate beyond the estimated error. Otherwise tallies would not be reliable. On the other hand, they are expected to carry some elements of randomness since they are Monte Carlo simulations. The repetitions run here shows acceptable behaviour. A point to note is that the number of particles started may depend on the available computer memory at the time of simulation.

The Neutron Cross Sections

The limiting factor of modern Monte Carlo codes lies in the cross sections uncertainties, particularly in the unresolved resonance range. For several important interactions no theoretical formulae of the neutron cross sections are known. Compilations of measurements are available but differ. Because of the wide variety of applications, no one set is superior. Moreover, isotopes of the same element often exhibit significant difference at the same neutron energy.

The measurements are further complicated by the sharp jumps inherent in the resonances, leading to unresolved resonances. Interpolations between different energies can be tricky and unreliable. In an example given by Levitt [LEV 72], there are approximately 33,000 resonances in the cross sections of ^{239}Pu . For each of the cross section (total, elastic scattering, inelastic scattering, capture, etc) and the corresponding energy, at least 8 points are required to describe each resonance adequately. One can thus imagine how demanding the computer storage can be.

The Fluence-to-Dose Conversion Factors

The conversion from neutron fluence into human biological dose equivalent rate was done using the NRPB-38 and the ICRP-21 conversion functions. These sets are not the only ones in existence. No one set is the best.

The exact absorbed dose is not computed here because the histories of the charged particles are not followed. Instead, the fluence is converted directly into dose equivalent using conversion factors. With the neutron fluence in particles/cm²-s, by multiplying with conversion factors in units of rem/hour per unit fluence, the converted answer would yield the dose equivalent in rem/hour.

It is said to be the consensus of the health physics community that the different conversion functions do not differ significantly for most applications where accuracy within $\pm 20\%$ is acceptable [JUD 97]. The differences between the various conversion functions may be due to source directionality, phantom geometry, penetration depth and the different neutron quality factors (which are primarily derived not from human subjects but animals) used.

The conversion functions are also subjected to revision by various national and international organisations such as the National Council on Radiation Protection and Measurements (NCRP), the International Commission on Radiological Protection (ICRP), the International Commission on Radiation Units and Measurements (ICRU), the American National Standards Institute (ANSI) and the American Nuclear Society (ANS).

The conversion factors contain the quality factors required to convert the absorbed dose in rads to rem. The ICRP and NCRP are currently considering an increase in the neutron quality factors by a factor of up to 2.5.

The conversion functions used are shown in Figure 5-5. In using step-wise functions for each energy bin instead of continuous conversion functions, a certain degree of accuracy is lost.

The continuous conversion function is shown in Figure 5-6. It can be seen that there are regions where the conversion is mere interpolation with no experimental base i.e. there exists energy regions of unknown values. The interpolation scheme deserves caution and should correspond to that recommended by the original publication. The ANSI/ANS publication, for example, recommends log-log interpolation. An inappropriate interpolation mode may yield large deviations.

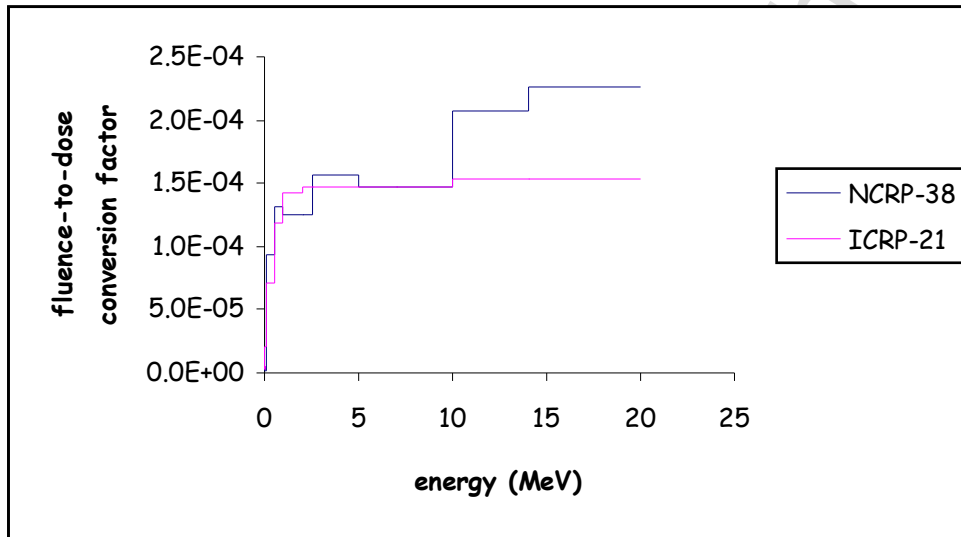


Figure 5-5. The NCRP-38 and the ICRP-21 conversion functions.

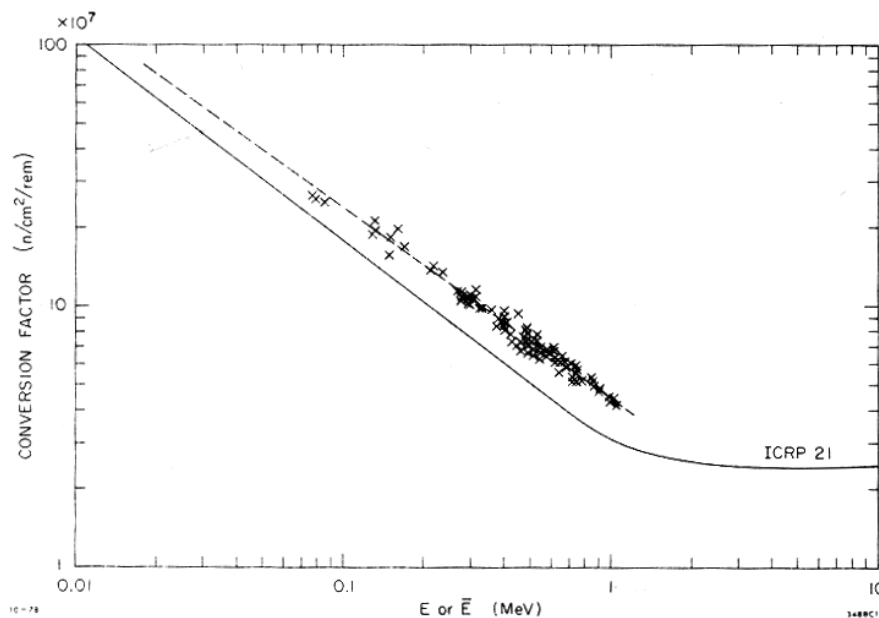


Figure 5-6. A continuous conversion function, [ICR 76]

Limitations of the model used in this work

The model constructed for simulation in this work deviates from the actual case in several aspects:

1. The MCNP 4B version on hand was not able to simulate any (γ, n) interaction. Thus the neutron source had to be a proxy.
2. A fission source was taken as proxy. In actual fact, the primary neutron spectrum is close, but not exactly similar, to that of a fission source. As shown in Figure 5-7, the original bump in the photoneutron spectrum suffers a smooth-out when it is represented by a fission source. This approximate resemblance is further lost as the neutrons penetrate the head shield. This is shown in Figure 5-8.

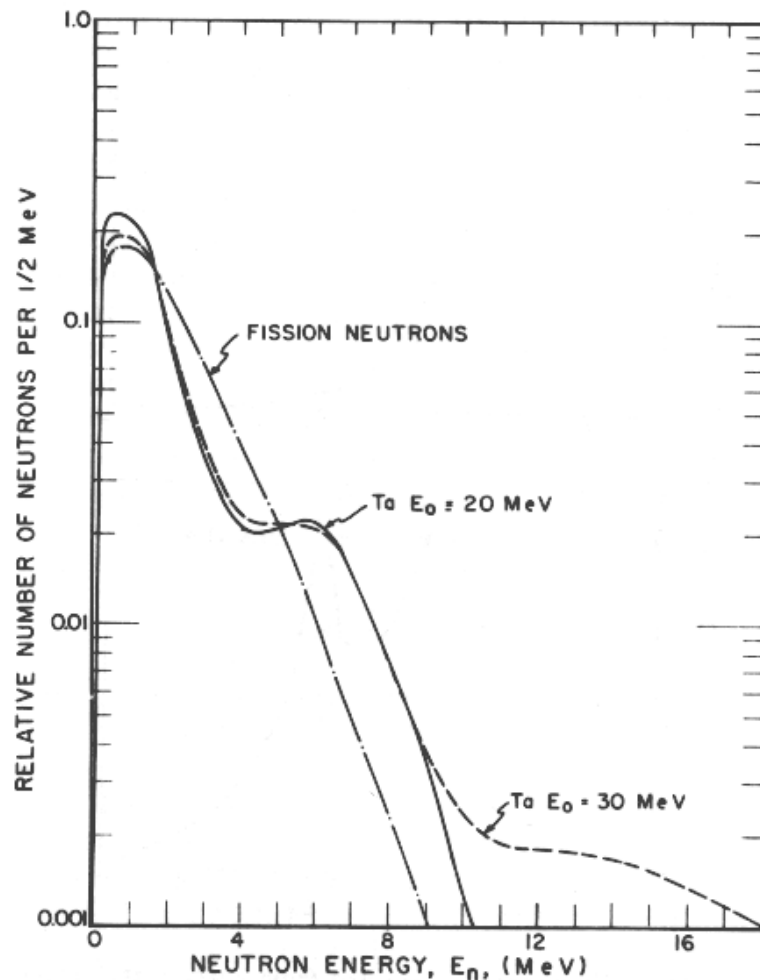


Figure 5-7. The primary photoneutron spectra for tantalum with peak bremsstrahlung energies E_0 . [NBS 64]

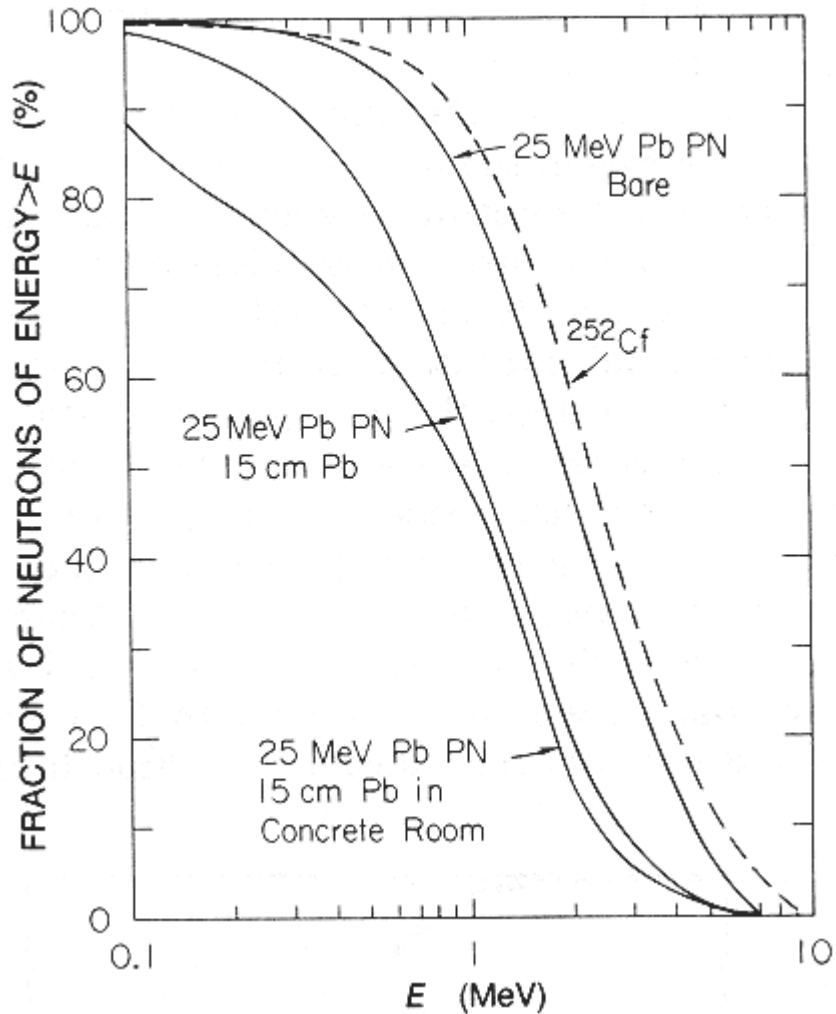


Figure 5-8. The neutron spectra after the modifying effects from the concrete room. 'PN' is for 'photoneutron'. [McC 79]

3. The fission source employed was bare, i.e. no head shield was present in the treatment room. Instead, the modifying effects of the head shield were demonstrated in a separate simulation. This was to avoid a deep penetration problem in MCNP, which time did not allow.
4. The isocentre was taken as the effective neutron source position. This is, however, not the only source of neutrons. The primary barrier and the patient also act as neutron sources.
5. An isotropic source was applied. This assumption is acceptable for neutrons emerging from the head shield since the initial angular distribution of the photoneutrons is destroyed by the time they emerge. In the case of taking the

patient of the walls as the neutron source, the angular distribution is expected to depend very much on the geometry involved.

6. A patient was absent as there was no time to simulate one and the geometry would have been over-complex. The neutron dose at the entrance is known to be higher if a patient and the couch are in place.
7. The walls were taken to be 100% concrete. The installation of power points, electrical supply, water pipes, electronic cables, etc. with the necessary compensators were not considered.

downloaded from www.marychin.org

Chapter 6. CONCLUSION

The double-bended maze design simulated in this work is characterised to have a tenth value length of 403.962 cm. The design achieved over 2 TVLs of dose equivalent attenuation. The dose equivalent at the entrance of the maze is found to be less than 0.5 mrem per hour, which equals to 5 μSv per hour. Estimations using the Kersey method yielded 8 μSv per hour. This empirical method clearly over-estimates dose equivalents at the entrance of the maze.

A similar maze design but with the second bend removed produced a dose equivalent of 9 μSv per hour, showing how important it is to employ a double-bended maze where possible. The dose equivalent at the entrance of the maze is also found to increase with increasing height.

It is proven that the fluence in the treatment room does not obey the inverse square law, due mainly to the scatter effect from the walls of the bunker.

A bare fission source is found to represent a medical electron linear accelerator with neutron source strengths 1) 2.25×10^{12} n Gy^{-1} x-ray at isocentre for a tungsten-shielded treatment head, or 2) 1.91×10^{12} n Gy^{-1} x-ray at isocentre for a lead-shielded head. These values approximate the Varian linac model C 1800 operating at 18 MeV.

The energy distribution is found to deviate from that of a fission source after the neutrons have penetrated the treatment head. The distribution is changed further as it traverses the passage of the maze, with a sharp depletion of the high energy components. From the neutrons found at the entrance of the maze, 19% have energy 0.025 eV or less, 73% have energy between 0.025 eV to 1 keV and 9% were fast (1 keV to 10 MeV).

The presence of secondary photons, not only in the treatment room but also at the entrance of the maze, is also demonstrated. The dose equivalent due to secondary photons is found to be about a ninth of that due to neutrons.

For neutrons, the NCRP-38 fluence-to-dose equivalent conversion factors are found to be more conservative than that of ICRP-21. For photons, the 1977 ANSI/ANS conversion factors appear to be more conservative compared to the ICRP-21 conversion factors.

In addition, the strengths and the difficulties of Monte Carlo simulations as opposed to conventional particle transport methods are also demonstrated. Monte Carlo simulation using the computer requires not only dedicated learning effort to pick up the technicalities of the code, but also considerable experience to master the art of variance reduction. Tallies do not work within a click of the mouse. The task is certainly more than just supplying the numbers and letting the computer do the rest. Moreover, reference materials are in most cases limited to the manual supplied along with the package, where many questions are left unanswered.

Simulation is not only subjected to the availability of the simulation software, but it also requires dedicated hardware facilities. Simulation time required can be extremely long and often, an overnight run may be far from adequate. Even when the user can afford to spare a generous length of simulation time, good tallies are never guaranteed. The user has to be prepared for disappointments that the tallies may or may not be successful, i.e. tallies that fail the statistical tests.

Simulation, on the other hand, offers wonderful flexibility over physical measurements. This flexibility is taken advantage of in this work, particularly in the section where a double-bended maze design was modified into a single-bended maze, which was done by tearing down a wall near the entrance of the maze and extending the other. Even more so in the section where different heights of the maze were considered. Both would have been too destructive and costly to be possible in an actual situation. Finding existing maze design with the desired configurations for study would be time-consuming and not feasible. In this work, all were done on a piece of computer.

Additionally, 'experiments' using simulations allow repetitions and extensions without the cautions against radiation exposure. Being able to isolate the secondary photons from the primary photons, as done in Chapter 4, is another advantage of simulation. This would be rather difficult to do experimentally.

downloaded from www.marychiro.org

APPENDIX A. Program Listing of Deterministic Simulation

```
//lead, 10MeV

#include <stdio.h>
#include <conio.h>
#include <math.h>

main()
{
    FILE *stream;
    const float Factor=0.981;
    int InitialEnergy=200;
    int InitialHeight=10000;
    int TotalGenerations=2090;
    int Emax,Emin,EmaxCurr,EminCurr;
    float FHeight;
    int G,a,b;
    float N[2][201];
    float GTotal;

    clrscr();
    stream=fopen("h:pb-10MeV.txt","w+");

    for(b=0;b<=InitialEnergy;b++)
        N[1][b]=0;
    G=0;
    Emax=InitialEnergy;
    Emin=InitialEnergy;
    N[1][InitialEnergy]=InitialHeight;
    do
    {
        G=G+1;
        GTotal=0;
        Emin=Emin*Factor;
        for(b=0;b<=InitialEnergy;b++)
        {
            N[0][b]=N[1][b];
            N[1][b]=0;
        };

        for(a=Emin;a<=Emax;a++)
        {
            EmaxCurr=a;
            EminCurr=a*Factor;
            FHeight=N[0][a]/(float)(EmaxCurr-EminCurr+1);
            for(b=EminCurr;b<=EmaxCurr;b++)
            {
                N[1][b]=N[1][b]+FHeight;
                GTotal=GTotal+FHeight;
            };
        };

        fprintf(stream,"\nG%d\t",G);
        for(b=0;b<=InitialEnergy;b++)
            fprintf(stream,"% .1f\t",N[1][b]);
        printf("\tTotal=%.1f\n",GTotal);
    }while(G<TotalGenerations);
    printf("That's all!");

    fclose(stream);
    return 0;
}
```

APPENDIX B. A Sample MCNP Input

```

continue
1 0 65 DXC:N IMP:N 0 $void
2 1 -2.43 51 -52 24 -37 1 -2 DXC:N .1 IMP:N 4 $left wall
3 1 -2.43 51 -52 24 -37 2 -3 DXC:N 1 IMP:N 2
4 1 -2.43 51 -52 24 -37 3 -4 DXC:N 1 IMP:N 2
5 1 -2.43 51 -52 24 -37 4 -5 DXC:N 2 IMP:N 2
6 1 -2.43 51 -52 24 -37 5 -6 DXC:N 2 IMP:N 2 $near of left wall
7 1 -2.43 51 -52 24 -31 7 -8 DXC:N 2 IMP:N 2 $near of middle wall
8 1 -2.43 51 -52 24 -31 8 -9 DXC:N 2 IMP:N 2
9 1 -2.43 51 -52 24 -31 9 -10 DXC:N 1 IMP:N 2
10 1 -2.43 51 -52 24 -31 10 -11 DXC:N 1 IMP:N 2
11 1 -2.43 51 -52 24 -31 11 -12 DXC:N 1 IMP:N 2 $middle wall
12 1 -2.43 51 -52 30 -37 13 -14 DXC:N 2 IMP:N 2 $near of right wall
13 1 -2.43 51 -52 30 -37 14 -15 DXC:N 1 IMP:N 2
14 1 -2.43 51 -52 30 -37 15 -16 DXC:N 1 IMP:N 4
15 1 -2.43 51 -52 30 -37 16 -17 DXC:N .1 IMP:N 4
16 1 -2.43 51 -52 30 -37 17 -18 DXC:N .1 IMP:N 4 $right wall
17 1 -2.43 48 -62 63 -64 19 -20 DXC:N .1 IMP:N 12 $supper bottom
18 1 -2.43 48 -62 63 -64 20 -21 DXC:N .1 IMP:N 12
19 1 -2.43 48 -62 63 -64 21 -22 DXC:N .1 IMP:N 8
20 1 -2.43 48 -62 63 -64 22 -23 DXC:N .1 IMP:N 8
21 1 -2.43 48 -62 63 -64 23 -24 DXC:N .1 IMP:N 8 $near of supper bottom
22 1 -2.43 51 -52 6 -7 24 -25 DXC:N .1 IMP:N 4 $bottom wall
23 1 -2.43 51 -52 6 -7 25 -26 DXC:N 1 IMP:N 2
24 1 -2.43 51 -52 6 -7 26 -27 DXC:N 1 IMP:N 2
25 1 -2.43 51 -52 6 -7 27 -28 DXC:N 2 IMP:N 2
26 1 -2.43 51 -52 6 -7 28 -29 DXC:N 2 IMP:N 2 $near of bottom wall
27 1 -2.43 51 -52 12 -18 24 -25 DXC:N .1 IMP:N 4 $entrance wall
28 1 -2.43 51 -52 12 -18 25 -26 DXC:N .1 IMP:N 4
29 1 -2.43 51 -52 12 -18 26 -27 DXC:N .1 IMP:N 4
30 1 -2.43 51 -52 12 -18 27 -28 DXC:N .1 IMP:N 2
31 1 -2.43 51 -52 12 -18 28 -29 DXC:N .1 IMP:N 2 $near of entrance wall
32 1 -2.43 51 -52 6 -13 32 -33 DXC:N 2 IMP:N 2 $near of top wall
33 1 -2.43 51 -52 6 -13 33 -34 DXC:N 2 IMP:N 2
34 1 -2.43 51 -52 6 -13 34 -35 DXC:N 1 IMP:N 2
35 1 -2.43 51 -52 6 -13 35 -36 DXC:N .1 IMP:N 2
36 1 -2.43 51 -52 6 -13 36 -37 DXC:N .1 IMP:N 4 $stop wall
37 1 -2.43 48 -62 63 -64 37 -38 DXC:N .1 IMP:N 8 $near of super top
38 1 -2.43 48 -62 63 -64 38 -39 DXC:N .1 IMP:N 8
39 1 -2.43 48 -62 63 -64 39 -40 DXC:N .1 IMP:N 8
40 1 -2.43 48 -62 63 -64 40 -41 DXC:N .1 IMP:N 12
41 1 -2.43 48 -62 63 -64 41 -42 DXC:N .1 IMP:N 12 $super top
42 3 -1.25 -43 -65 DXC:N .1 IMP:N 4 $soil
43 3 -1.25 43 -44 -65 DXC:N .1 IMP:N 4
44 3 -1.25 44 -45 -65 DXC:N .1 IMP:N 4
45 3 -1.25 45 -46 -65 DXC:N .1 IMP:N 4
46 3 -1.25 46 -47 -65 DXC:N .1 IMP:N 4
47 3 -1.25 47 -48 -65 DXC:N 1 IMP:N 4 $near of soil
48 1 -2.43 48 -49 1 -18 24 -37 DXC:N 1 IMP:N 4 $floor
49 1 -2.43 49 -50 1 -18 24 -37 DXC:N 2 IMP:N 2
50 1 -2.43 50 -51 1 -18 24 -37 DXC:N 2 IMP:N 2 $near of floor
51 1 -2.43 52 -53 1 -18 24 -37 DXC:N 2 IMP:N 2 $near of ceiling
52 1 -2.43 53 -54 1 -18 24 -37 DXC:N 2 IMP:N 2
53 1 -2.43 54 -55 1 -18 24 -37 DXC:N 2 IMP:N 2
54 1 -2.43 55 -56 1 -18 24 -37 DXC:N 1 IMP:N 2
55 1 -2.43 56 -57 1 -18 24 -37 DXC:N .1 IMP:N 4 $ceiling
56 1 -2.43 57 -58 63 -64 24 -37 DXC:N .1 IMP:N 8 $near of super ceiling
57 1 -2.43 58 -59 63 -64 24 -37 DXC:N .1 IMP:N 8
58 1 -2.43 59 -60 63 -64 24 -37 DXC:N .1 IMP:N 8
59 1 -2.43 60 -61 63 -64 24 -37 DXC:N .1 IMP:N 12
60 1 -2.43 61 -62 63 -64 24 -37 DXC:N .1 IMP:N 12 $super ceiling
61 2 -1.225E-3 51 -52 6 -7 29 -32 #70 DXC:N 2 IMP:N 1 $room air
62 2 -1.225E-3 51 -52 7 -12 31 -32 DXC:N 2 IMP:N 1 $turn air
63 2 -1.225E-3 51 -52 12 -13 30 -32 #71 DXC:N 2 IMP:N 2 $passage air
64 2 -1.225E-3 51 -52 12 -66 29 -30 #72 DXC:N .1 IMP:N 2 $entrance air
65 2 -1.225E-3 -65 #1 #2 #3 #4 #5 #6 #7 #8 #9 #10 #11 #12 #13 #14 #15 &
#16 #17 #18 #19 #20 #21 #22 #23 #24 #25 #26 #27 #28 #29 #30 #31 #32 #33 &
#34 #35 #36 #37 #38 #39 #40 #41 #42 #43 #44 #45 #46 #47 #48 #49 #50 #51 &
#52 #53 #54 #55 #56 #57 #58 #59 #60 #61 #62 #63 #64 #70 #71 #72 &
DXC:N .1 IMP:N 8 $outside air
70 2 -1.225E-3 -70 DXC:N .1 IMP:N 1
71 2 -1.225E-3 -71 DXC:N 1 IMP:N 1
72 2 -1.225E-3 -72 DXC:N .1 IMP:N 2

1 PX -500 $left wall
2 PX -480
3 PX -460
4 PX -440
5 PX -420

```

6 PX -400 \$left wall
7 PX 400 \$middle wall
8 PX 420
9 PX 440
10 PX 460
11 PX 480
12 PX 500 \$middle wall
13 PX 700 \$right wall
14 PX 720
15 PX 740
16 PX 760
17 PX 780
18 PX 800 \$right wall
19 PY -600 \$supper bottom
20 PY -580
21 PY -560
22 PY -540
23 PY -520
24 PY -500 \$supper bottom - bottom wall
25 PY -480
26 PY -460
27 PY -440
28 PY -420
29 PY -400 \$bottom wall
30 PY -200
31 PY 200
32 PY 400 \$top wall
33 PY 420
34 PY 440
35 PY 460
36 PY 480
37 PY 500 \$top wall - super top
38 PY 520
39 PY 540
40 PY 560
41 PY 580
42 PY 600 \$super top
43 PZ -310 \$soil
44 PZ -290
45 PZ -270
46 PZ -250
47 PZ -230
48 PZ -210 \$soil - floor
49 PZ -190
50 PZ -170
51 PZ -150 \$floor
52 PZ 150 \$ceiling
53 PZ 170
54 PZ 190
55 PZ 210
56 PZ 230
57 PZ 250 \$ceiling - super ceiling
58 PZ 270
59 PZ 290
60 PZ 310
61 PZ 330
62 PZ 350 \$super ceiling
63 PX -200
64 PX 200
65 SX 150 1000
66 PX 900
70 S 200 100 0 10
71 S 600 300 0 10
72 S 800 -300 0 10

```

SDEF ERG=D1
SP1 -2 1.2895
E14 .025E-6 1E-6 1E-3 .1 1 10 20
F14:N 70
F24:N 70
F34:N 70
DXT:N 200 100 0 11 11 1E3 1E-4
DE24 2.5e-8 1e-7 1e-6 1e-5 1e-4 1e-3 1e-2 1e-1 5e-1 1 2.5 5 7 10 14 20
DF24 3.67e-6 3.67e-6 4.46e-6 4.54e-6 4.18e-6 3.76e-6 3.56e-6 2.17e-5 &
9.26e-5 1.32e-4 1.25e-4 1.56e-4 1.47e-4 1.47e-4 2.08e-4 2.27e-4
DE34 2.5e-8 1e-7 1e-6 1e-5 1e-4 1e-3 1e-2 1e-1 5e-1 1 2 5 10 20
DF34 3.85e-6 4.17e-6 4.55e-6 4.35e-6 4.17e-6 3.7e-6 3.57e-6 2.08e-5 &
7.14e-5 1.18e-4 1.43e-4 1.47e-4 1.47e-4 1.54e-4
M1 1001 .0093 $H concrete
8016 .0463 $O
14000 .00992 $Si
20000 .00883 $Ca
6000 .0065 $C
M2 7014 78.09 $N air
8016 20.95 $O
18000 .93 $Ar
M3 1001 16.87 $H soil
8016 27 $O
13027 1.976 $Al
14000 8.963 $Si
CTME 300

```

downloaded from www.marychin.org

REFERENCES

- Booth TE, A sample problem for variance reduction in MCNP, Los Alamos National Laboratory (1985)
- Forster A, Video reel #11, "Relative errors, figure of merit" from MCNP workshop, Los Alamos National Laboratory (1983) as given in [BOO85]
- Greene D, Williams PC, Linear accelerators for radiation therapy 2nd ed, IOP, Bristol (1985)
- Judith FB ed, MCNP - A general Monte Carlo N-Particle transport code, Los Alamos National Laboratory report, LA-12625-M (1997)
- Kersey RW, Estimation of neutron and gamma radiation doses in the entrance mazes of SL75-20 linear accelerator treatment rooms, *Medicamundi*, 24, 151-5 (1979)
- Knoll GF, Radiation detection and measurement 2nd ed, Willey, New York (1989)
- Krane KS, Introductory nuclear physics, Wiley, Chichester (1988)
- Lalonde R, The effect of neutron-moderating materials in higher-energy linear accelerator mazes, *Phys. Med. Biol.*, 42, 335-344 (1997)
- Levitt LB, The probability table method for treating unresolved resonances in Monte Carlo calculations, *Nucl. Sci. Eng.*, 49, 450 (1972) as given in [LUX 91]
- Lewis RD, An MCNP-based model of a linear accelerator x-ray beam, *Phys. Med. Bio.*, 44, 1219-1230 (1999)
- Lux I, Koblinger L, Monte Carlo particle transport methods: neutron and photon calculations, CRC Press, Boca Raton (1991)
- McCall RC, Jenkins TM, Shore RA, Transport of accelerator produced neutrons in a concrete room, *IEEE Trans. Nuc. Sci.*, NS-26, 1, 1593-1602 (1979)
- McCall RC, Neutron yield of medical electron accelerators SLAC-PUB 4480, Stanford Linear Accelerator Centre, Stanford (1987) as given in [McG 88]
- McGinley PH, Neutron contamination of x-ray beams produced by the Varian Clinac 1800, *Phys Med Biol*, 34, 6, 777-783 (1989)
- McGinley PH, Evaluation of neutron dose equivalent levels at the maze entrance of medical accelerator treatment rooms, *Med Phys*, 18, 2, 279-281 (1991)
- McGinley PH, Photoneutron fields in medical accelerator rooms with primary barriers constructed of concrete and metals, *Health Physics*, 63, 6, 698-701 (1992)

NBS handbook 97, Shielding for high-energy electron accelerator installations, National Bureau of Standards, (1964)

NBS handbook 63, Protection against neutron radiation up to 30 million electron volts, National Bureau of Standards, (1967)

NCRP report no 38, Protection against neutron radiation, National Council on Radiation Protection and Measurements (1971)

NCRP report no 49, Structural shielding design and evaluation for medical use of x rays and gamma rays of energies up to 10 MeV, National Council on Radiation Protection and Measurements (1976)

NCRP report no 79, Neutron contamination from medical electron accelerators, National Council on Radiation Protection and Measurements (1984)

ICRP publications 15 and 21, Protection against ionizing radiation from external sources and Data for protection against ionizing radiation from external sources, Pergamon, Oxford (1976)

Swanson WP, Calculation of neutron yields released by electrons incident on selected materials, *Health Physics*, 35, 353 (1978) as given in [NCR 84]

Swanson WP, Improved calculation of phtoneutron yield released by incident electrons, *Health Physics*, 37, 347 (1979) as given in [NCR 84]

downloaded from www.industrydocuments.ucsf.edu/docs/0909